J. Fluid Mech. (2004), *vol.* 518, *pp.* 1–34.
DOI: 10.1017/S0022112004000539 Printed in the United Kingdom

Resonance oscillations with thermal effects of an inviscid gas in a closed tube

By A. GOLDSHTEIN†, A. ALEXEEV AND C. GUTFINGER

Faculty of Mechanical Engineering, Technion – Israel Institute of Technology, Haifa 32000, Israel

(Received 10 July 2003 and in revised form 11 May 2004)

The problem of gas motion inside a resonance tube, closed at one end by a plug and fitted at the other with an oscillating piston is treated analytically and numerically. An analytical model is derived for arbitrary piston motion and gas oscillations about the first resonance frequency, where the gas flow is characterized by a shock wave travelling periodically back and forth in the tube. The model is obtained by a perturbation analysis in terms of a small-amplitude parameter ε. All the hydrodynamic properties of the gas are predicted with accuracy up to the second-order terms of ε. Isentropic and adiabatic problem formulations are addressed. Expressions for spatial distributions of the time-averaged hydrodynamic gas properties are derived for any frequency within the resonance band. It is shown that they are determined by the gas adiabatic exponent γ and the law that governs the motion of the piston. The analytical model is verified by comparison with a numerical solution, showing good agreement.

1. Introduction

The present paper deals with modelling of thermal processes caused by gas oscillations in a closed tube, which were described by Sprenger (1954), Saenger & Hudson (1960) and Merkli & Thomann (1975*b*). The authors of the first two papers have found in their experiments that travelling shock waves result in an increase in the average temperature and pressure at the closed end of the tube, while the authors of the last paper demonstrated that not only heating, but also cooling is possible in the tube, where standing acoustic waves are generated.

In the work of Merkli & Thomann (1975*b*), the first analytical treatment for the energy transport processes was given. Previous treatments of this problem in acoustic oscillations in a tube were restricted to overall energy balances (see e.g. Betchov 1958; Gulyaev & Kuznetsov 1963; Temkin 1968). Merkli & Thomann (1975*b*) explained the unusual distribution of the heat flux within the so-called resonance tube, i.e. a tube closed at one end by a plug and fitted at the other with an oscillating piston. The key to the understanding of this distribution is in the existence of 'thermoacoustic streaming', a phenomenon which is analogous to the acoustic streaming first described by Rayleigh (1945). Thermoacoustic streaming is a second-order effect, which describes the time-averaged heat flux associated with wall friction. Lawrenson *et al.* (1998) have shown that a proper choice of the geometric shape of a resonator can significantly amplify the transport processes, which are important for such industrial applications as thermoacoustic engines, refrigerators, etc.

† Present address: MediGuide Ltd., P.O.B. 15003, Haifa 31053, Israel.

A review of linear acoustic streaming (including thermal effects in boundary layers) was presented by Riley (1997). Riley (2001) and Riley & Trinh (2001) demonstrated that a non-conservative oscillating force may induce streaming even within an inviscid fluid.

The aforementioned papers by Merkli & Thomann (1975*b*) and Lawrenson *et al.* (1998), as well as a more recent publication by Ilinskii, Lipkens & Zabolotskaya (2001), are limited to small driving amplitudes and frequencies far enough from the resonance in order to prevent shock waves. These restrictions are probably useful for industrial applications, but do not allow the description of particularly prominent heat effects, which are of fundamental interest. Since the works of Merkli & Thomann (1975*b*) and Saenger & Hudson (1960), neither experimental nor computational results have been presented on the temperature or pressure gradients that can be produced by weak shock waves in gas columns at resonance. The theoretical paper by Goldshtein *et al.* (1996) concerning these phenomena is restricted to the special case of a fixed sinusoidal driving frequency and isentropic conditions. These restrictions, which are inherent for the analytical method of Goldshtein *et al.* (1996), limit the applicability of the model. The purpose of the present work is to obtain a basic understanding of the thermal processes occurring in gas oscillations accompanied by weak shock waves, and to develop efficient mathematical tools that are free from the above restrictions.

In general, there are three basic phenomena affecting the thermal processes: nonlinearity, viscous damping, and heat interactions with the tube. A consistent theory accounting for the first two of these phenomena was first proposed by Chester (1964). He expanded the solution in a series of a small-amplitude parameter ε, which is of the order of the square root of the ratio of the piston amplitude, $\tilde{l}$, and the tube length, $\tilde{L}$, and showed that a combination of the first- and second-order solutions satisfies the boundary conditions. Moreover, Chester's solution predicts the growth of the gas oscillation amplitude and the transition from a continuous acoustic wave to a shock wave, when the driving frequency is inside the resonance band. The approach developed by Chester turned out to be extremely effective and was later modified by several authors (Rott 1974; Keller 1976). The works by Ilgamov *et al.* (1996) and Goldshtein *et al.* (1996) present a detailed discussion of other relevant studies.

Comparison of Chester's theory with experiments (see Ilgamov *et al.* 1996; Alexeev, Goldshtein & Gutfinger 2002) showed that the model deviation from experiments increases with the amplitude parameter, ε. At amplitudes $\varepsilon \geqslant 0.1$ all existing theories become unsatisfactory. Aganin, Ilgamov & Smirnova (1996) hypothesized that the discrepancy between models and experiments may arise due to the effect of energy dissipation on shock waves, which was not included in the models. More recently, numerical simulations by Alexeev *et al.* (2002) have shown that heat interaction with the tube wall strongly affects gas flow for frequencies within the resonance band. They proposed a phenomenological model, accounting for heat interaction in turbulent flows, which provides good agreement with experimental data. The principal aim of the present work is to develop an analytical model of resonance oscillations of a gas in a closed tube, which is valid for the 'large' amplitudes characterized by $0.1 \leqslant \varepsilon < 0.3$, and to verify the model numerically.

In the present work, we extend the model of Chester to account for temperature, pressure and density distributions along the tube axis due to nonlinearity and for energy input by the vibrating piston. In order to understand the effect of thermal interactions with the walls, we consider an adiabatic model of gas oscillations. The adiabatic model assumes perfectly insulated walls, leading to an increase in temperature due to energy dissipation by the shocks. Aiming to obtain a closed-form analytical

solution of the problem, we simplify our theory by neglecting viscous effects. Since in real experiments, resonance flow is strongly affected by viscous and heat interactions, a quantitative comparison of an inviscid theoretical model with experimental data is hardly possible. Hence, we develop a numerical model complementary to our theory, and use the numerical solutions to verify the analytical model.

The paper is organized as follows. In § 2, we formulate the basic equations for isentropic and adiabatic gas models, with the corresponding conditions on the shock wave and boundary conditions for an arbitrary periodic piston motion. The generalization of the sinusoidal law of piston motion, which was used in previous theoretical papers, allows us to approximate more closely the experimental conditions characterized by larger amplitudes (see e.g. Gulyaev & Kuznetsov 1963; Sturtevant 1974; Shuster *et al.* 2002). In order to obtain a self-consistent solution of the problem, we introduce the global mass conservation condition (see Goldshtein *et al.* 1996). The solution of the problem is expanded in a series of the small parameter ε up to terms of the second order.

In § 3, we present the analytical solution of the problem. The first-order solution is reduced to the problem of free gas oscillation with an initial distribution having a jump. We show that the general solution of this problem can be expressed via an arbitrary function, say $f(x)$, which is defined on an interval of double the tube length. Analysing the second-order solution, we derive a general equation for the arbitrary function $f(x)$. This equation is a generalization of Chester's famous equation for sinusoidal piston motion to the case of arbitrary periodic piston motion. Its analytic solution is discussed in § 3.3. A solution of the second-order problem is defined with accuracy to an arbitrary function, which could be obtained from the condition of solvability of the third-order problem. Rather than doing that, we verify the accuracy of this approximate solution by comparison with the numerical solution of the problem. In § 4, we introduce a numerical method used to obtain the solution of the hydrodynamic equations.

In § 5, we discuss the properties of the derived analytical solution and compare them with the results of numeric simulations. In § 5.1, we rewrite the analytic solution in the characteristic form and compare it with Chester's solution. The comparison shows that the global mass conservation condition and conditions on the shock wave, which are omitted in Chester's model, lead to the appearance of additional second-order terms in the Riemann invariants. These terms are responsible for the second-order time-averaged distributions of gas density, temperature and pressure along the tube. It is shown that the distribution of the hydrodynamic properties is controlled by the adiabatic exponent and the law of piston motion. The mathematical model of the thermal processes is of fundamental and practical interest, since it shows how to reach a desirable distribution of a hydrodynamic property. In § 5.2, we show that the energy input by the piston is dissipated by the travelling shock waves. This energy balance condition, which was used by Betchov (1958) and Temkin (1968) for the closure of their models, is identically satisfied in our model. At the end of § 5, we derive an analytical model of adiabatic gas heating by the shock wave, and consider the effects of gas viscosity and thermal conductivity, which create spatial gradients of the time-averaged gas properties. We summarize our results in § 6.

2. Statement of the problem

2.1. *Basic equations*

We consider a tube of length $\tilde{L}$ closed at one end by a rigid plug and at the other by an oscillating piston. The tube is filled by a perfect gas. For the sake of simplicity,

we neglect the gas viscosity. We impose homogeneous initial conditions, i.e. an initial state of the gas which is described by a constant density $\tilde{\rho}_0$, pressure $\tilde{P}_0$, temperature $\tilde{\theta}_0$ and speed of sound $\tilde{C}_0 = \sqrt{\gamma \tilde{P}_0/\tilde{\rho}_0}$. The equations of one-dimensional motion of an inviscid perfect gas are

$$\frac{\partial \tilde{\rho}}{\partial \tilde{t}} + \frac{\partial \tilde{\rho}\tilde{u}}{\partial \tilde{x}} = 0, \tag{1a}$$

$$\frac{\partial \tilde{u}}{\partial \tilde{t}} + u\frac{\partial \tilde{u}}{\partial \tilde{x}} + \frac{1}{\tilde{\rho}}\frac{\partial \tilde{P}}{\partial \tilde{x}} = 0, \tag{1b}$$

$$\frac{\partial \tilde{P}}{\partial \tilde{t}} + \tilde{u}\frac{\partial \tilde{P}}{\partial \tilde{x}} + \gamma \tilde{P}\frac{\partial \tilde{u}}{\partial \tilde{x}} = \tilde{q}_0, \tag{1c}$$

where $\tilde{t}$ is time, $\tilde{x}$ is the axial coordinate, $\gamma = \tilde{c}_p/\tilde{c}_v$ is the isentropic exponent, $\tilde{c}_v$ and $\tilde{c}_p$ being the specific heats of the gas at constant volume and pressure, respectively. Moreover, $\tilde{\rho}$, $\tilde{u}$, $\tilde{P}$ and $\tilde{\theta}$ are the gas density, velocity, pressure and temperature, respectively. An equation of state of a perfect gas is given by

$$\tilde{P} = \tilde{R}\tilde{\rho}\tilde{\theta}, \quad \tilde{R} = \tilde{k}\tilde{m}, \tag{2a,b}$$

where $\tilde{k} = 1.3806 \times 10^{-23}$ J K^{-1} is the same constant for all gases and $\tilde{m}$ is the molecular mass of the gas. Most papers deal with flows in which the entropy is constant everywhere: these are referred to as homentropic flows. To define a homentropic flow the volumetric energy supply per unit time should be specified. When $\tilde{q}_0$ is negative, the heat is removed from the tube by external cooling. Such cooling is necessary if one wants to sustain periodic gas oscillations accompanied by shock waves, which dissipate mechanical energy into heat. On the other hand, when $\tilde{q}_0 = 0$, the generated heat is accumulated inside the tube leading to an increase in time-averaged gas temperature. We call the problem adiabatic, when $\tilde{q}_0 = 0$.

The energy dissipated in a shock wave is

$$\tilde{E}_{sh} = \tilde{\theta}\Delta\tilde{S}, \tag{3}$$

where $\Delta\tilde{S}$ is the entropy increase due to irreversible processes. We limit our consideration to the case of weak shock waves, for which the pressure jump across the shock is much smaller than the initial pressure, $\Delta\tilde{P} \ll \tilde{P}_0$. When shock waves are weak, the entropy increase over a shock is of order $(\Delta\tilde{P}/\tilde{P}_0)^3$ and equals

$$\Delta\tilde{S} = \tilde{c}_v \frac{\gamma - 1}{12\gamma^2}\left(\frac{\Delta\tilde{P}}{\tilde{P}_0}\right)^3. \tag{4}$$

When $\Delta\tilde{P}/\tilde{P}_0 \ll 1$, one can neglect the irreversibility due to shocks and replace the energy conservation equation (1c) by the following isentropic relation:

$$\tilde{P} = \tilde{P}_0\left(\frac{\tilde{\rho}}{\tilde{\rho}_0}\right)^{\gamma}. \tag{5}$$

We consider a long tube closed by a solid plug at $\tilde{x} = 0$ and by an oscillating piston at $\tilde{x} = \tilde{L}$. The motion of the piston is periodic with a period $\tilde{T}$ and amplitude $\tilde{l}$, such that the piston coordinate at any time is given by

$$\tilde{x}_p(\tilde{t}) = \tilde{L} + \tilde{l}x_p^{(2)}[\tilde{\omega}(\tilde{t} - \tilde{t}_*)]. \tag{6a}$$

Here, $\tilde{\omega} = 2\pi/\tilde{T}$ is the angular frequency of the oscillation, parameter $\tilde{t}_*$ defines the initial position of the piston, and $x_p^{(2)}(\alpha)$ is a dimensionless periodical function with

period 2π and zero average:

$$x_p^{(2)}(\alpha) = x_p^{(2)}(\alpha + 2\pi), \tag{6b}$$

$$\int_0^{2\pi} x_p^{(2)}(\alpha)\,\mathrm{d}\alpha = 0. \tag{6c}$$

Without any loss of generality, one can define this function in such a way that $x_p^{(2)}(0)$ corresponds to the instroke position of the piston

$$x_p^{(2)}(0) = x_{in}^{(2)}, \tag{6d}$$

where $x_{in}^{(2)} \equiv \min_{\alpha} x_p^{(2)}(\alpha)$. In the majority of works dealing with gas oscillations in a resonance tube, a sinusoidal law of piston motion is adopted in the form

$$x_p^{(2)}(\alpha) = -\cos\alpha. \tag{7}$$

In many experiments, however, especially with larger vibrational amplitudes, a crank mechanism is used for gas excitation. In a crank mechanism, the law of piston motion $x_p^{(2)}(\alpha)$ differs from that given by (7). A more accurate description can be written (Shigley & Uicker 1995) as

$$x_p^{(2)}(\alpha) = -\cos\alpha + \frac{\sqrt{1-(\lambda\sin\alpha)^2}}{\lambda} - \frac{2E(\lambda^2)}{\lambda\pi}, \tag{8}$$

where $E(\lambda)$ is the complete elliptic integral of the second kind, and λ is a parameter which characterizes the ratio of the crank radius and the connecting-rod length, and is usually smaller than $1/3$. Due to the properties of $E(\lambda)$, equation (8) satisfies conditions (6*b*, *c*). The latter model is more general than the one given by (7) and approaches it in the limit $\lambda \to 0$. In the present study, we derive a solution for the general function $x_p^{(2)}(\alpha)$, and all the results are illustrated for the particular laws of piston motion given by equations (7) and (8).

The boundary conditions of the problem can be written in the form

$$\tilde{u}(\tilde{t}, \tilde{x}) = 0 \quad \text{at} \quad \tilde{x} = 0, \tag{9a}$$

$$\tilde{u}(\tilde{t}, \tilde{x}) = \tilde{u}_p(\tilde{t}) \quad \text{at} \quad \tilde{x} = \tilde{x}_p(\tilde{t}), \tag{9b}$$

where $\tilde{u}_p(\tilde{t}) = \mathrm{d}\tilde{x}_p(\tilde{t})/\mathrm{d}\tilde{t}$ is the speed of the piston. We consider the resonance problem when the piston angular frequency is within a resonance band about the first linear resonance frequency $\tilde{\omega}_{res} = 2\pi/\tilde{T}_{res}$, where $\tilde{T}_{res} = 1/f_{res} = 2\tilde{L}/\tilde{C}_0$ is the resonance period. According to this definition, the resonance period is equal to the time taken for the shock propagating with the speed of sound to travel along the tube backwards and forwards. The particular case of strictly resonance oscillations, i.e. $\tilde{\omega} = \tilde{\omega}_{res}$, was analysed by Betchov (1958) and Goldshtein *et al.* (1996). The purpose of the present paper is to extend this analysis to the whole resonance band, in which gas oscillations are accompanied by periodic shock waves. Calculation of the bounds of the resonance band is one of our tasks.

Since the problem includes a shock wave, a jump condition on the shock front should be imposed. For an inviscid perfect gas, this jump condition can be written in the form

$$\tilde{\rho}_l(\tilde{U} - \tilde{u}_l) = \tilde{\rho}_r(\tilde{U} - \tilde{u}_r), \tag{10a}$$

$$\tilde{\rho}_l(\tilde{U} - \tilde{u}_l)^2 + \tilde{P}_l = \tilde{\rho}_r(\tilde{U} - \tilde{u}_r)^2 + \tilde{P}_r, \tag{10b}$$

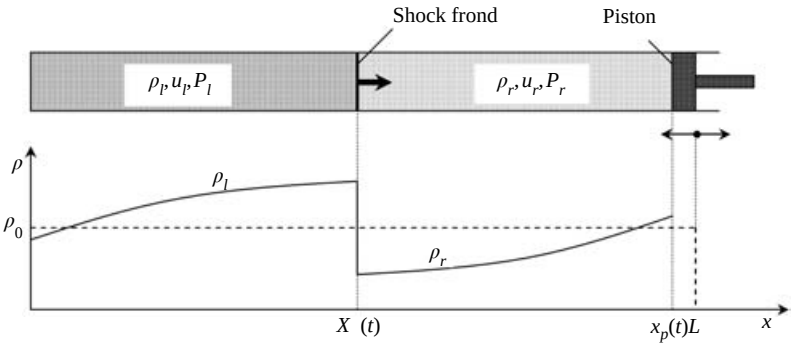

FIGURE 1. Schematic of a resonance tube with global mass conservation condition.

$$\frac{\tilde{P}_l}{\tilde{\rho}_l} - \frac{\tilde{P}_r}{\tilde{\rho}_r} + \frac{\gamma - 1}{2}\left(\frac{1}{\tilde{\rho}_l} - \frac{1}{\tilde{\rho}_r}\right)(\tilde{P}_r + \tilde{P}_l) = 0, \tag{10c}$$

where $\tilde{X}$ is the shock position, $\tilde{U}$ is the speed of shock propagation, and indexes l and r denote the values at the left and right sides of the shock, respectively (see figure 1).

Usually the jump condition is enough to define the position of the shock front. However, in the case of a resonance tube, an additional condition is needed. For example, Galiev, Ilgamov & Sadykov (1970) used a condition of time-averaged mass conservation at any cross-section of the tube. In the present study, we use a condition of global mass conservation within the tube. In our notation, this condition can be written (see figure 1) as

$$\int_0^{\tilde{X}(\tilde{t})} \tilde{\rho}_l(\tilde{t}, \tilde{x})\,\mathrm{d}\tilde{x} + \int_{\tilde{X}(\tilde{t})}^{\tilde{x}_p(\tilde{t})} \tilde{\rho}_r(\tilde{t}, \tilde{x})\,\mathrm{d}\tilde{x} = \tilde{\rho}_0 \tilde{L}. \tag{11}$$

We now formulate several different mathematical models of the resonance problem. We define the model given by equations (1a,b), (5), and conditions (10a,b), (11) as isentropic. This definition differs from that used in most of the previous papers, which considered a simplified version of this model in which conditions (10a,b), (11) were disregarded. The effect of the shock wave and global mass conservation conditions on isentropic resonance gas oscillations is discussed in § 5.1.

The relevance of the isentropic model to experiments is not obvious, since it disregards all irreversible processes occurring during gas oscillations. These processes can significantly modify the flow, especially for long times. However, due to the asymptotic nature of resonance oscillations, the isentropic model can be extended to describe a physically more realistic situation by accounting for heat production, and thermal and viscous interactions between gas and tube wall. It follows from equations (3), (4) that the heat produced by a weak shock wave is of order ε^3, and defined by terms of order ε. This means that the first-order solution of the isentropic problem can serve as a basis for the calculation of external cooling $\tilde{q}_0$, which removes the energy dissipated by the shock and preserves the periodic nature of gas oscillations (see § 5.2). We call such a flow pseudo-isentropic.

Solutions of the isentropic model can be used to mimic an adiabatic process, which occurs when the tube walls are perfectly insulated. Adiabatic resonance oscillations are non-periodic due to continuous gas heating. Strictly speaking, the adiabatic model is given by equations (1a–c) with $\tilde{q}_0 = 0$, and shock conditions (10a–c). However,

isentropic relation (5) satisfies equation (1*c*) and condition (10*c*) with accuracy of ε^2. Equation (10*c*) is more general than equations (3), (4), which hold for weak shock waves only. For the case of weak shocks both are identical with accuracy of ε^3. We also note that gas oscillations and gas heating by shock waves have different time scales: the first process occurs for a period of $\tilde{T}_{res}$, and the second for $\tilde{T}_{res}\varepsilon^{-2}$. This prompts the idea of modelling the adiabatic process as a superposition of two processes: rapid gas oscillations, which are accompanied by slow heat production in the gas. A simple analytical model of heat production in an adiabatic gas is discussed in § 5.3.

Let us define the following dimensionless variables and functions:

$$x = \tilde{x}/\tilde{L}, \quad t = \tilde{t}\tilde{C}_0/\tilde{L}, \quad u = \tilde{u}/\tilde{C}_0, \quad \rho = \tilde{\rho}/\tilde{\rho}_0, \quad P = \tilde{P}/\left(\tilde{\rho}_0\tilde{C}_0^2\right). \tag{12}$$

Hence, the dimensionless tube length L, initial density, ρ_0, and speed of sound, C_0, are equal to unity, while the dimensionless period of resonance oscillations $T_0 = 2$ and the dimensionless initial pressure $P_0 = 1/\gamma$.

The general solution of the problem of resonance gas oscillations includes a discontinuity. We are looking for a solution consisting of two continuous parts separated by a shock front (see figure 1). We call the solution at the left of the shock the left-side wave solution and at the right of the shock the right-side wave solution. Moreover, we denote all hydrodynamic properties describing these left-side and right-side waves by indexes l and r, respectively. Using (1*a*, *b*), the isentropic relation (5) and the dimensionless values (12), one obtains the equations of motion of the continuous parts as follows:

$$\frac{\partial \rho_\beta}{\partial t} + \rho_\beta \frac{\partial u_\beta}{\partial x} + u_\beta \frac{\partial \rho_\beta}{\partial x} = 0, \tag{13a}$$

$$\frac{\partial u_\beta}{\partial t} + u_\beta \frac{\partial u_\beta}{\partial x} + \rho_\beta^{\gamma-2} \frac{\partial \rho_\beta}{\partial x} = 0. \tag{13b}$$

Here, index β stands for either l or r. Boundary conditions (9*a*, *b*) in dimensionless form are

$$u_l(t, x) = 0 \quad \text{at} \quad x = 0, \tag{14a}$$

$$u_r(t, x) = u_p(\tau) \quad \text{at} \quad x = x_p(\tau), \tag{14b}$$

where the piston coordinate $x_p(\tau)$ and speed $u_p(\tau)$ are

$$x_p(\tau) = 1 + \varepsilon^2 \frac{x_p^{(2)}(\alpha)}{\pi}, \tag{15a}$$

$$u_p(\tau) = \frac{T_0}{T}\varepsilon^2 \frac{\mathrm{d}}{\mathrm{d}\alpha} x_p^{(2)}(\alpha), \tag{15b}$$

$$\alpha = \pi(\tau - \tau_*). \tag{15c}$$

Here, $\tau = tT_0/T$, $\tau_* = t_*T_0/T$ and $\varepsilon = \sqrt{\pi\tilde{l}/\tilde{L}}$, while $x_p(\tau)$ and $u_p(\tau)$ are periodic functions with a period T_0. We restrict the analysis to the small piston amplitudes $\tilde{l} \ll \tilde{L}$, which implies that the parameter ε is small, $\varepsilon \ll 1$. Smallness of ε allows us to investigate the resonance problem by expanding the hydrodynamic equations (Chester 1964) and the subsidiary conditions (Goldshtein *et al.* 1996) in appropriate series.

Using (5) together with (12), we rewrite the jump conditions (10*a*, *b*) and global mass conservation condition (11) in dimensionless form as

$$\rho_l(U - u_l) = \rho_r(U - u_r), \tag{16a}$$

$$\rho_l(U-u_l)^2+\rho_l^{\gamma}/\gamma=\rho_r(U-u_r)^2+\rho_r^{\gamma}/\gamma, \tag{16b}$$

$$\int_0^{X(t)}\rho_l(t,x)\,\mathrm{d}x+\int_{X(t)}^{x_p(t)}\rho_r(t,x)\,\mathrm{d}x=1. \tag{17}$$

As mentioned earlier, condition (16*b*) is accurate up to the second order, while (16*a*) and (17) are always accurate.

Experiments show that resonance gas oscillations in closed tubes are periodic with a period T equal that of piston oscillations. We impose this periodicity condition on the solution of the resonance problem such that

$$\Gamma(t,x)=\Gamma(t+T,x), \tag{18}$$

where Γ denotes any gas property. Now the isentropic problem of resonance gas oscillations can be formulated as a solution of (13), which satisfies to the boundary conditions (14), the conditions at the shock front (16), the global mass conservation condition (17) and the periodicity condition (18).

A solution of the resonance problem, which is obtained by the perturbation method, is discussed in the following subsections.

2.2. *Perturbation method*

We expand all hydrodynamic properties in series with respect to a small parameter ε. For the case of isentropic flow characterized by (5), the series for the hydrodynamic density, velocity, pressure and temperature can be written as follows:

$$\rho_\beta(\tau,x)=1+\varepsilon\rho_\beta^{(1)}(\tau,x)+\varepsilon^2\rho_\beta^{(2)}(\tau,x), \tag{19a}$$

$$u_\beta(\tau,x)=\varepsilon u_\beta^{(1)}(\tau,x)+\varepsilon^2 u_\beta^{(2)}(\tau,x), \tag{19b}$$

$$P_\beta(\tau,x)=\frac{1}{\gamma}+\varepsilon\rho_\beta^{(1)}(\tau,x)+\varepsilon^2\left[\rho_\beta^{(2)}(\tau,x)+\frac{\gamma-1}{2}\left(\rho_\beta^{(1)}(\tau,x)\right)^2\right], \tag{19c}$$

$$\theta_\beta(\tau,x)=\frac{1}{\gamma}+\varepsilon\frac{\gamma-1}{\gamma}\left[\rho_\beta^{(1)}(\tau,x)+\varepsilon\rho_\beta^{(2)}(\tau,x)+\varepsilon\frac{\gamma-2}{2}\left(\rho_\beta^{(1)}(\tau,x)\right)^2\right]. \tag{19d}$$

For the sake of simplicity, we express all the hydrodynamic properties in the above equations as functions of τ rather than t. In terms of τ, the periodicity condition (18) is simplified to

$$\Gamma(\tau,x)=\Gamma(\tau+2,x). \tag{20}$$

Saenger & Hudson (1960) showed that the increase of gas oscillation amplitude and the transition from continuous acoustic waves to shock waves occurs when the driving frequencies are close to the linear resonance frequency. The band of driving frequencies for which an oscillating shock wave appears is called the resonance band. Calculation of the width of the resonance band is one of the goals of our paper. When viscous effects are disregarded, the only parameter affecting the width of the band is ε. We assume that the period of the piston oscillations T is close to the resonance period T_0, and expand T in a series of the small parameter ε as follows:

$$T=T_0+\varepsilon T_1=2+\varepsilon T_1. \tag{21}$$

We show below that the detuning parameter T_1 delineates the resonance band with an error of the order of ε^3 rather than ε^2.

Substitution of expansions (19*a*, *b*) into (13) yields
first order of ε

$$\frac{\partial u_\beta^{(1)}(\tau, x)}{\partial \tau} + \frac{\partial \rho_\beta^{(1)}(\tau, x)}{\partial x} = 0, \tag{22a}$$

$$\frac{\partial \rho_\beta^{(1)}(\tau, x)}{\partial \tau} + \frac{\partial u_\beta^{(1)}(\tau, x)}{\partial x} = 0; \tag{22b}$$

second order of ε

$$\frac{\partial u_\beta^{(2)}(\tau, x)}{\partial \tau} + \frac{\partial \rho_\beta^{(2)}(\tau, x)}{\partial x} = \varphi\left(u_\beta^{(1)}, \rho_\beta^{(1)}\right), \tag{23a}$$

$$\frac{\partial \rho_\beta^{(2)}(\tau, x)}{\partial \tau} + \frac{\partial u_\beta^{(2)}(\tau, x)}{\partial x} = \psi\left(u_\beta^{(1)}, \rho_\beta^{(1)}\right), \tag{23b}$$

where

$$\varphi\left(u_\beta^{(1)}, \rho_\beta^{(1)}\right) = \frac{T_1}{2}\frac{\partial u_\beta^{(1)}(\tau, x)}{\partial \tau} - u_\beta^{(1)}\frac{\partial u_\beta^{(1)}(\tau, x)}{\partial x} - (\gamma - 2)\rho_\beta^{(1)}\frac{\partial \rho_\beta^{(1)}(\tau, x)}{\partial x}, \tag{23c}$$

$$\psi\left(u_\beta^{(1)}, \rho_\beta^{(1)}\right) = \frac{T_1}{2}\frac{\partial \rho_\beta^{(1)}(\tau, x)}{\partial \tau} - \rho_\beta^{(1)}\frac{\partial u_\beta^{(1)}(\tau, x)}{\partial x} - u_\beta^{(1)}\frac{\partial \rho_\beta^{(1)}(\tau, x)}{\partial x}. \tag{23d}$$

Expansion of the boundary conditions (14) leads to

first order of ε

$$u_l^{(1)}(\tau, 0) = 0, \tag{24a}$$

$$u_l^{(1)}(\tau, 1) = 0; \tag{24b}$$

second order of ε

$$u_l^{(2)}(\tau, 0) = 0, \tag{25a}$$

$$u_r^{(2)}(\tau, 1) = \dot{x}_p^{(2)}[\pi(\tau - \tau_*)]. \tag{25b}$$

Additionally, one can expand the dimensionless shock wave speed, $U(\tau)$, and the coordinate of the shock front, $X(\tau)$, in the following series:

$$U(\tau) = U^{(0)}(\tau) + \varepsilon U^{(1)}(\tau), \tag{26a}$$

$$X(\tau) = X^{(0)}(\tau) + \varepsilon X^{(1)}(\tau). \tag{26b}$$

Here, we drop the second-order terms, since they do not affect the solution of (22) and (23). At the zeroth order, the speed of the shock is $U^{(0)}(\tau) = 1$ for a shock wave travelling from the left to the right of the tube, and $U^{(0)}(\tau) = -1$ for a shock wave travelling in the opposite direction. The piston motion is described by (15) in terms of ε^2 and, apparently, does not affect gas oscillations at the zeroth- and first-order approximations. Hence, in the zeroth-order approximation, the speed of the shock front is equal to ± 1 and the trajectory of the shock front is a zigzag line as shown in figure 2. Choosing the time of the shock wave reflection from the plug as the initial time, one can write $X(\tau)$ in the form

$$X(\tau) = \begin{cases} \tau + \varepsilon X^{(1)}(\tau), & 0 < \tau < 1, \\ -\tau + \varepsilon X^{(1)}(\tau), & -1 < \tau < 0. \end{cases} \tag{27a}$$

Since, $X(\tau)$ is a periodic function with a period 2, it can be periodically continued for $\tau < -1$ and $\tau > 1$. In particular, the shock wave reflects from the plug ($x = 0$)

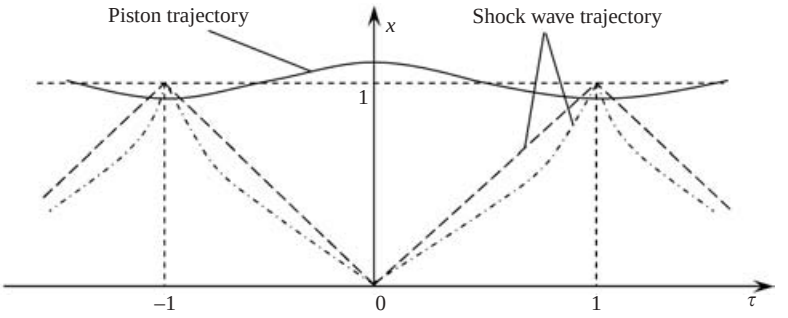

FIGURE 2. Space–time diagram of resonance oscillations for different approximations of a shock wave trajectory. The dashed lines indicate the zero-order approximation, while the dashed-dotted lines indicate the first-order approximation.

at $\tau_{pl} = \pm 2, \pm 4, \pm 6 \ldots$ and from the piston ($x = 1$) at $\tau_p = \pm 1, \pm 3, \pm 5 \ldots$. Hence, $X^{(1)}(\tau)$ does not affect τ_{pl} and τ_p, as shown in figure 2, and only distorts the shock wave trajectory. Taking into account the relations between the shock coordinate and velocity, one can obtain from (27a) the following equation for the shock velocity:

$$U(\tau) = \begin{cases} 2/T + \varepsilon \dfrac{\mathrm{d}}{\mathrm{d}\tau} X^{(1)}(\tau), & 0 < \tau < 1, \\ -2/T + \varepsilon \dfrac{\mathrm{d}}{\mathrm{d}\tau} X^{(1)}(\tau), & -1 < \tau < 0. \end{cases} \tag{27b}$$

Equations (27a, b) define the shock wave coordinate and speed, respectively, with second-order accuracy.

After substitution of (15) and (26b) into the global mass conservation condition (17), we obtain density conservation conditions $\rho_\beta^{(1)}$ and $\rho_\beta^{(2)}$ as follows:

$$\int_0^{X^{(0)}} \rho_l^{(1)}(\tau, x)\,\mathrm{d}x + \int_{X^{(0)}}^1 \rho_r^{(1)}(\tau, x)\,\mathrm{d}x = 0, \tag{28a}$$

$$\int_0^{X^{(0)}} \rho_l^{(2)}(\tau, x)\,\mathrm{d}x + \int_{X^{(0)}}^1 \rho_r^{(2)}(\tau, x)\,\mathrm{d}x = -\frac{1}{\pi} x_p^{(2)}[\pi(\tau - \tau_*)] + X^{(1)}(\tau)\left[\rho_l^{(1)}(\tau, x) - \rho_r^{(1)}(\tau, x)\right]_{x = X^{(0)}(\tau)}. \tag{28b}$$

Expansion (19a) is normalized in such a way that the total mass of the gas is accounted for in the term of zeroth order of ε. Hence, each perturbation of the homogeneous solution, given by the zeroth-order approximation, does not affect the total mass of the gas. Equations (28a, b) merely express this fact for the first and second orders of ε. The right-hand side of the first-order equation (28a) is equal to zero, while in the second-order equation (28b), the right-hand side has two terms, which account for the piston motion and shock acceleration.

Substitution of the series from (19a, b) and (26a, b) into the jump conditions (16) yields at $x = X^{(0)}(\tau)$:

first order of ε

$$U^{(0)}(\tau)\rho_l^{(1)}(\tau, x) - u_l^{(1)}(\tau, x) = U^{(0)}(\tau)\rho_r^{(1)}(\tau, x) - u_r^{(1)}(\tau, x); \tag{29a}$$

second order of ε

$$\begin{aligned} &U^{(0)}(\tau)\rho_l^{(2)}(\tau,x)-u_l^{(2)}(\tau,x)+\rho_l^{(2)}(\tau,x)\big[U^{(1)}(\tau)-u_l^{(1)}(\tau,x)\big]\\ &\quad+X^{(1)}(\tau)\frac{\partial}{\partial x}\big[U^{(1)}(\tau)\rho_l^{(2)}(\tau,x)-u_l^{(1)}(\tau,x)\big]\\ &=U^{(0)}(\tau)\rho_r^{(2)}(\tau,x)-u_r^{(2)}(\tau,x)+\rho_r^{(2)}(\tau,x)\big[U^{(1)}(\tau)-u_r^{(1)}(\tau,x)\big]\\ &\quad+X^{(1)}(\tau)\frac{\partial}{\partial x}\big[U^{(1)}(\tau)\rho_r^{(2)}(\tau,x)-u_r^{(1)}(\tau,x)\big] \end{aligned} \tag{29b}$$

where

$$U^{(1)}(\tau)=\frac{\gamma-1}{4}\big[\rho_l^{(1)}(\tau,x)+\rho_r^{(1)}(\tau,x)\big]U^{(0)}(\tau)+\frac{1}{2}\big[u_l^{(1)}(\tau,x)+u_r^{(1)}(\tau,x)\big]. \tag{29c}$$

3. Solution of the problem

3.1. *First-order solution*

In this section, we discuss a general solution of (22) with the boundary conditions (24) and condition (29*a*) at the shock front. Following Chester (1964), we look for a solution that is a combination of those for two continuous waves, one on the left and one on the right side of the shock. Such a solution can be expressed via an arbitrary function $f(x)$, say, which is defined on an interval $-1<x<1$ and has two continuous derivatives within this interval. The solution of (22) with conditions (24) and (29*a*) is given as follows:

for the right-side wave

$$u_r^{(1)}(\tau,x)=f'(\tau+x-1)-f'(\tau-x+1), \tag{30a}$$

$$\rho_r^{(1)}(\tau,x)=-f'(\tau+x-1)-f'(\tau-x+1); \tag{30b}$$

for the left-side wave

$$u_l^{(1)}(\tau,x)=\begin{cases} f'(\tau+x-1)-f'(\tau-x-1), & 0<\tau<1,\\ f'(\tau+x+1)-f'(\tau-x+1), & -1<\tau<0, \end{cases} \tag{30c}$$

$$\rho_l^{(1)}(\tau,x)=\begin{cases} -f'(\tau+x-1)-f'(\tau-x-1), & 0<\tau<1,\\ -f'(\tau+x+1)-f'(\tau-x+1), & -1<\tau<0. \end{cases} \tag{30d}$$

To specify $f(x)$, we use the global mass conservation condition (28*a*). Substitution of (30*b*) and (30*d*) into (28*a*) and integration yields

$$f(1)-f(-1)=0. \tag{31}$$

It follows from this result that the average value of $f'(x)$ over one period is zero. This property was postulated by Chester (1964), and, as shown above, is a consequence of the global mass conservation condition.

We now discuss the physical meaning of the function $f'(x)$ appearing (30). Let continuous functions $u_l^{(1)}(-1,x)$ and $\rho_l^{(1)}(-1,x)$ be the gas velocity and density distributions at time $\tau=-1$. With these functions and (30*c*, *d*), $f'(x)$ is expressed as

$$f'(x)=\big[u_l^{(1)}(-1,x)-\rho_l^{(1)}(-1,x)\big]/2, \tag{32a}$$

$$f'(-x)=-\big[u_l^{(1)}(-1,x)+\rho_l^{(1)}(-1,x)\big]/2. \tag{32b}$$

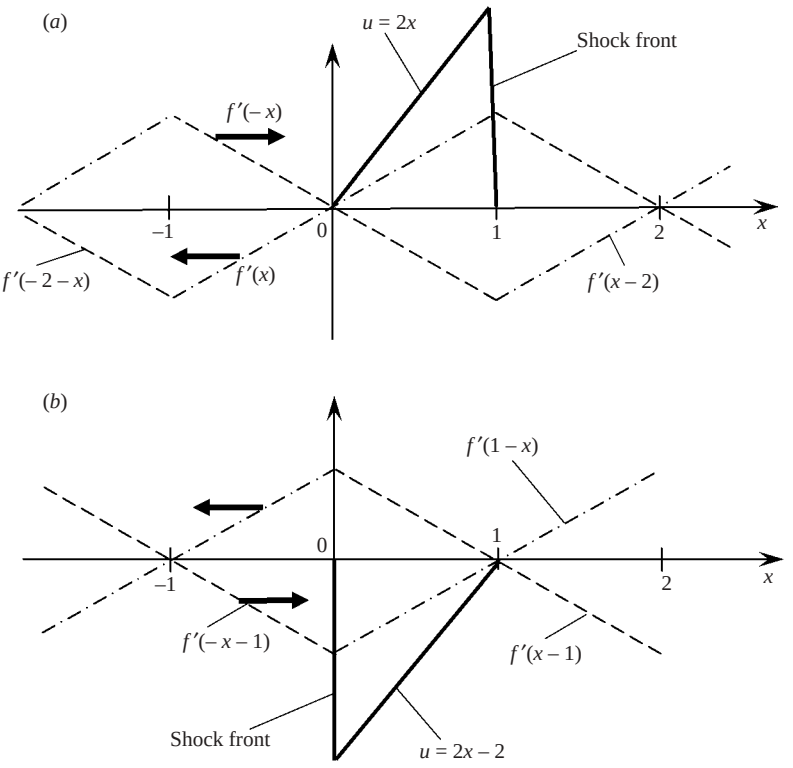

FIGURE 3. Gas motion at resonance as predicted by solution $(30a, c)$ for the special case of $f(x) = x^2/2$. (*a*) $\tau = -1$, (*b*) $\tau = 0$.

These relations show that the function $f'(x)$ is determined completely and unambiguously by the initial conditions of the problem and vice versa. Since $u_l^{(1)}(-1, x)$ and $\rho_l^{(1)}(-1, x)$ are continuous within the interval $[0, 1]$, the function $f'(x)$ has no jumps in the intervals $[0, 1]$ and $[-1, 0]$. For $f'(x)$ to be continuous in the interval $[-1, 1]$, it is required that $\lim_{x\to 0} u_l^{(1)}(-1, x) = 0$. Imposing a similar condition at $x = 1$, i.e. $\lim_{x\to 1} u_l^{(1)}(-1, x) = 0$, leads to $f'(1) = f'(-1)$, which holds for a solution without discontinuities. Hence, the function $f'(x)$ should be periodic with a period of 2. The solution of such a problem can be found in many textbooks describing free oscillations without shocks of a gas confined between two rigid walls.

We are now looking for a solution with a discontinuity for which $f'(1) \neq f'(-1)$. Equation (30) provides a generalization of the classical solution for the case of an initial condition with a discontinuity. It is valid for a single period and may be extended to larger times by periodical continuation. We illustrate the solution with the example of a parabolic function $f(x) = x^2/2$, leading to $f'(x) = x$ defined on $-1 < x < 1$. We consider the velocity at a fixed time $\tau = -1$. At this moment, the function is continued periodically by profiles $f'(x + 2n)$ and $f'(-x + 2n)$, where $n = \pm 1, \pm 2, \ldots$ (see figure 3*a*). Solution $(30a, c)$ on the segment $0 < x < 1$, corresponding to the tube length, is expressed via four functions $f'(\tau + x - 1)$, $f'(\tau - x + 1)$, $f'(\tau + x + 1)$ and $f'(\tau - x - 1)$, which degenerate for $\tau = -1$ into profiles $f'(x - 2)$, $f'(-x)$, $f'(x)$, and $f'(-2 - x)$ shown in figure 3(*a*). Functions depicted by dashed lines move in the positive direction, while those depicted by

dash-dotted lines in the negative direction. All these functions propagate with the speed of sound. As shown, the discontinuity representing the shock front is at the tube end, $x=1$, and the left-side solution (30*c*) describes the gas velocity everywhere in the tube. From (30*c*), one obtains for $\tau=-1$ the gas velocity along the tube as $u=2x$, shown by the solid line in figure 3(*a*). As the time τ increases, the profiles propagate along the x-axis. The arrows in figure 3(*a*) show the direction of the profile propagation.

During the time interval $-1<\tau<0$, profiles $f'(\tau+x-1)$ and $f'(\tau+x+1)$ propagating in the negative direction describe a velocity jump, $\Delta u=2$ moving in the same direction. The continuous part of the velocity is described by the function $f'(\tau-x+1)$, moving in the positive direction. At $\tau=0$, the discontinuity is located at $x=0$ as seen in figure 3(*b*). At this moment, the right-side solution (30*a*) describes the gas velocity along the whole tube as $u=2x-2$. During the time interval $0<\tau<1$, the functions $f'(\tau+x-1)$, $f'(\tau-x+1)$ and $f'(\tau-x-1)$ constitute the solution (30*a*, *c*). At $\tau=0$, these functions degenerate into the profiles $f'(x-1)$, $f'(1-x)$ and $f'(-1-x)$ depicted in figure 3(*b*). The second profile contributes to the continuous part of the solution only, while the others generate the shock wave, which propagates in the positive x-direction. At $\tau=1$, when the shock wave reaches $x=1$, the profiles are identical to those at $\tau=-1$ (figure 3*a*) and the motion repeats itself.

Substitution of (30) and (27*a*) into the jump condition (29*c*) yields the following expression for $U^{(1)}$:

$$U^{(1)}(\tau)=\begin{cases}\dfrac{3-\gamma}{2}f'(2\tau-1)-\dfrac{\gamma+1}{4}[f'(1)+f'(-1)], & 0<\tau<1,\\[2ex] \dfrac{3-\gamma}{2}f'(2\tau+1)+\dfrac{\gamma+1}{4}[f'(1)+f'(-1)], & -1<\tau<0.\end{cases}\tag{33}$$

Comparing this expression with (27*b*) and using (21), we express T_1 and $X^{(1)}$ via the function $f(x)$ as

$$T_1=\frac{\gamma+1}{2}[f'(1)+f'(-1)],\tag{34a}$$

$$\frac{\mathrm{d}X^{(1)}\tau}{\mathrm{d}\tau}=\begin{cases}\dfrac{3-\gamma}{2}f'(2\tau-1), & 0<\tau<1,\\[2ex] \dfrac{3-\gamma}{2}f'(2\tau+1), & -1<\tau<0.\end{cases}\tag{34b}$$

In order to obtain $X^{(1)}$, equation (34*b*) should be integrated with a zero initial condition, since the shock wave reflects from the plug at $\tau=0$. After integration, we obtain

$$X^{(1)}(\tau)=\begin{cases}\dfrac{3-\gamma}{4}[f(2\tau-1)-f(-1)], & 0<\tau<1,\\[2ex] \dfrac{3-\gamma}{4}[f(2\tau+1)-f(1)], & -1<\tau<0.\end{cases}\tag{35}$$

Due to the property (31), $X^{(1)}$ vanishes at the instant of shock reflection from the walls, i.e. at $\tau=-1, 0, 1$. For simplicity and without loss of generality, we assume

$$f(1)=f(-1)=0.\tag{36}$$

Equations (30), (33)–(36) yield the first-order general solution of the problem described by (22), (24), (28*a*) and (29*a*). This solution is expressed via an unknown function $f'(x)$, which is determined in the following subsection.

3.2. *Second-order solution*

We introduce the following variables:

$$z = \tau + x - 1, \tag{37a}$$

$$y = \tau - x + 1 \tag{37b}$$

and rewrite the solution given by (30) in the form

$$u_r^{(1)}(y,z) = f'(z) - f'(y), \tag{38a}$$

$$\rho_r^{(1)}(y,z) = -f'(z) - f'(y), \tag{38b}$$

$$u_l^{(1)}(y,z) = \begin{cases} f'(z) - f'(y-2), & 0 < \tau < 1, \\ f'(z+2) - f'(y), & -1 < \tau < 0, \end{cases} \tag{38c}$$

$$\rho_l^{(1)}(y,z) = \begin{cases} -f'(z) - f'(y-2), & 0 < \tau < 1, \\ -f'(z+2) - f'(y), & -1 < \tau < 0. \end{cases} \tag{38d}$$

Variables y and z are the leading-order terms in the expansion of the characteristics, as shown in § 5.1, below.

We turn to the equations governing the second approximation of the solution. The first-order solution (38a, b) can be combined with (23) to yield the following equations for the right-side wave:

$$\frac{\partial}{\partial z}\left[u_r^{(2)}(y,z) + \rho_r^{(2)}(y,z)\right] = \frac{\varphi(y,z) + \psi(y,z)}{2}, \tag{39a}$$

$$\frac{\partial}{\partial y}\left[u_r^{(2)}(y,z) - \rho_r^{(2)}(y,z)\right] = \frac{\varphi(y,z) - \psi(y,z)}{2}, \tag{39b}$$

where

$$\varphi(y,z) = (3-\gamma)[f'(y)f''(z) - f'(z)f''(y)] + (\gamma - 1)[f'(y)f''(y) - f'(z)f''(z)] - \frac{T_1}{2}[f''(y) - f''(z)] \tag{39c}$$

$$\psi(y,z) = 2f'(y)f''(y) + 2f'(z)f''(z) - \frac{T_1}{2}[f''(y) + f''(z)]. \tag{39d}$$

The equations for the left-side wave can be obtained by substitution of variables $\{y-2, z\}$ for $0 < \tau < 1$ and $\{y, z+2\}$ for $-1 < \tau < 0$ instead of the variables $\{y, z\}$ into (39). Hence, the left-side wave solution is

$$\frac{\partial}{\partial z}\left[u_l^{(2)}(y,z) + \rho_l^{(2)}(y,z)\right] = \begin{cases} [\varphi(y-2,z) + \psi(y-2,z)]/2, & 0 < \tau < 1, \\ [\varphi(y,z+2) + \psi(y,z+2)]/2, & -1 < \tau < 0, \end{cases} \tag{40a}$$

$$\frac{\partial}{\partial y}\left[u_l^{(2)}(y,z) - \rho_l^{(2)}(y,z)\right] = \begin{cases} [\varphi(y-2,z) - \psi(y-2,z)]/2, & 0 < \tau < 1, \\ [\varphi(y,z+2) - \psi(y,z+2)]/2, & -1 < \tau < 0. \end{cases} \tag{40b}$$

It is important to note that (39a, b) and (40a, b) are independent and can be integrated over y and z. Therefore, an analytical solution for these equations can be obtained up to unknown functions of y and z. The unknown functions can be found through the conditions of the second-order approximation. The condition at the shock wave front (29b) can be expressed in terms of the variables y and z from (33)–(38) as

$$\left[\rho_r^{(2)} - u_r^{(2)}\right] - \left[\rho_l^{(2)} - u_l^{(2)}\right] = \left(\frac{3-\gamma}{4}\right)[f'(1) - f'(-1)][2f'(z) + f'(1) + f'(-1)], \quad y = 1, \tag{41a}$$

$$\left[\rho_r^{(2)} + u_r^{(2)}\right] - \left[\rho_l^{(2)} + u_l^{(2)}\right] = \left(\frac{3-\gamma}{4}\right)[f'(1) - f'(-1)][2f'(y) + f'(1) + f'(-1)], \quad z = 1. \tag{41b}$$

The periodicity condition (20) reduces to

$$\rho_l^{(2)}\big|_{\tau=-1} = \rho_l^{(2)}\big|_{\tau=1}, \tag{42a}$$

$$u_l^{(2)}\big|_{\tau=-1} = u_l^{(2)}\big|_{\tau=1}. \tag{42b}$$

For the global mass conservation condition (28*b*), we obtain

$$\int_0^{\pm\tau} \rho_l^{(2)}(\tau, x)\,\mathrm{d}x + \int_{\pm\tau}^{1} \rho_r^{(2)}(\tau, x)\,\mathrm{d}x = -\frac{1}{\pi} x_p^{(2)}[\pi(\tau - \tau_*)] + \left(\frac{3-\gamma}{4}\right)[f'(1) - f'(-1)][f'(2\tau \pm 1) - f'(-1)], \tag{43}$$

where the plus sign stands for $0 < \tau < 1$, while the minus sign is for $-1 < \tau < 0$. A solution of the problem (39) and (40) can be presented in the following form:

$$u_r^{(2)} = \Psi(x, y, z) + \frac{T_1}{2}[(\tau - 1)f''(z) - (\tau + 1)f''(y)], \tag{44a}$$

$$\rho_r^{(2)} = \Omega(x, y, z) - \frac{T_1}{2}[(\tau - 1)f''(z) + (\tau + 1)f''(y)], \tag{44b}$$

$$u_l^{(2)} = \begin{cases} \Psi(x, y-2, z) + \dfrac{T_1}{2}(\tau - 1)[f''(z) - f''(y)], & 0 < \tau < 1, \\ \Psi(x, y, z+2) + \dfrac{T_1}{2}(\tau + 1)[f''(z) - f''(y)], & -1 < \tau < 0, \end{cases} \tag{44c}$$

$$\rho_l^{(2)} = \begin{cases} \Omega(x, y-2, z) - \dfrac{T_1}{2}(\tau - 1)[f''(z) + f''(y)], & 0 < \tau < 1, \\ \Omega(x, y, z+2) - \dfrac{T_1}{2}(\tau + 1)[f''(z) + f''(y)], & -1 < \tau < 0, \end{cases} \tag{44d}$$

where

$$\Psi(x, y, z) = \frac{(3-\gamma)}{4}[f(y)f''(z) - f(z)f''(y)] + \frac{(3-\gamma)}{8}[f'(y)f''(y) - f'(z)f''(z)] + \frac{(\gamma+1)}{2}x[f'(y)f''(y) - f'(z)f''(z)], \tag{44e}$$

$$\Omega(x, y, z) = \frac{(3-\gamma)}{4}[2f'(y)f'(z) - f(z)f''(y) - f(y)f''(z)] + \frac{(3-\gamma)}{8}[f'(z)f'(z) - f'(y)f'(y)] + \frac{(\gamma+1)}{2}x[f'(y)f''(y) - f'(z)f''(z)] + C_\rho. \tag{44f}$$

Here, C_ρ is a constant to be evaluated. Equation (44) satisfies the condition at the shock front (41), the boundary condition at the plug (25*a*) and the periodicity condition (42).

Substitution of (44a, c, e) into (25b) leads to the following equation for the unknown function $f'(\tau)$;

$$(\gamma+1)f'(\tau)f''(\tau) - T_1 f''(\tau) = \dot{x}_p^{(2)}[\pi(\tau-\tau_*)]. \tag{45}$$

This equation was derived and solved by Chester (1964) for the particular case of piston motion given by (7). Another expression for the function f can be obtained by substitution of (44b, d, f) into global mass conservation condition (43) and integration leading to

$$\frac{\gamma+1}{2}\left[f'(\tau) - \frac{T_1}{\gamma+1}\right]^2 = \frac{x_p^{(2)}[\pi(\tau-\tau_*)]}{\pi} + E, \tag{46a}$$

where

$$E = C_\rho - \frac{T_1^2}{2(\gamma+1)} + \frac{\gamma+5}{4}K, \tag{46b}$$

$$K = \frac{1}{2}\int_{-1}^{1}\left[f'(t)\right]^2 \mathrm{d}t. \tag{46c}$$

We note that (46) is an integral of (45), with E being the integration constant. Due to the use of condition (43), the integration constant is expressed in terms of parameters C_ρ and E, the physical meanings of which are addressed in the next subsection.

3.3. *Solution of the Chester equation*

Now we use (46) to calculate the constant C_ρ from (44f). Integrating (46a) over the period $[-1, 1]$ and taking into account (6c), (36) and (46b), we obtain the constant C_ρ as

$$C_\rho = \frac{T_1^2}{\gamma+1} + \frac{\gamma-3}{4}K. \tag{47}$$

Now, we show that the constant E in (46a) can be expressed in terms of the piston's instroke position $x_{in}^{(2)}$ of (6d) as

$$E = \left|x_{in}^{(2)}\right|/\pi. \tag{48}$$

The left-hand side of (46a) is essentially non-negative, which requires that $E \geqslant |x_{in}^{(2)}|/\pi$. We look for a solution including a shock wave, which implies $f'(1) \neq f'(-1)$. Taking into account that a shock wave propagates from the higher to the lower pressure, we impose the following condition:

$$f'(1) - f'(-1) > 0. \tag{49}$$

Bearing this in mind, a solution of (46) can be obtained as follows:

$$f'(\tau) = \begin{cases} \dfrac{T_1}{\gamma+1} + \dfrac{A}{2}\sqrt{\Delta x_p(\tau)}, & \tau_* \leqslant \tau \leqslant 1, \\ \dfrac{T_1}{\gamma+1} - \dfrac{A}{2}\sqrt{\Delta x_p(\tau)}, & -1 \leqslant \tau \leqslant \tau_*, \end{cases} \tag{50a}$$

where

$$\Delta x_p(\tau) = \frac{x_p^{(2)}[\pi(\tau-\tau_*)] - x_{in}^{(2)}}{2}, \tag{50b}$$

and the constant A is defined as

$$A = \frac{4}{\sqrt{\pi(\gamma+1)}}. \tag{50c}$$

Equation (48) provides continuity of the solution (50) at $\tau = \tau_*$ corresponding to the piston instroke position, since $\Delta x_p(\tau_*) = 0$ (see (6d)). As $(\mathrm{d}x_p^{(2)}(\alpha)/\mathrm{d}\alpha)|_{\alpha=0} = 0$, the

derivative of the solution exists at $\tau = \tau_*$ providing a smooth connection between the left and right parts of the solution at this point, and, hence, smoothness of $f'(\tau)$ over the period $[-1, 1]$. Note that substitution of the solution (50) into (34*a*) for T_1 turns it into an identity.

By definition, τ_* is equal to the lag between the instant of the shock reflection from the plug and the instant when the piston is at its instroke position. Experiments show that this lag unambiguously characterizes a frequency within the resonance band (Saenger & Hudson 1960). Hence, the period of resonance oscillations can be expressed as a function of τ_*, i.e. $T = T(\tau_*)$. To derive such a function, we need to calculate $T_1(\tau_*)$ (see (21)). To this end, we integrate $f'(\tau)$ given by (50) over the period $[-1, 1]$ and taking into account (31) obtain

$$T_1(\tau_*) = \frac{A(\gamma+1)}{4}\left[\int_{-1}^{\tau_*}\sqrt{\Delta x_p(\tau)}\,\mathrm{d}\tau - \int_{\tau_*}^{1}\sqrt{\Delta x_p(\tau)}\,\mathrm{d}\tau\right]. \tag{51}$$

Substitution of this equation and (50) into (46*b*) and integration over $[-1, 1]$ leads to

$$K = -\frac{T_1^2}{(\gamma+1)^2} + \frac{2}{\pi(\gamma+1)}\left|x_{in}^{(2)}\right|. \tag{52}$$

Equations (51) and (52) can be substituted into (47) to obtain C_ρ as a function of the parameter τ_*.

The solution (50), (51) defines the first-order terms of hydrodynamic variables via (38) unambiguously, while the second-order terms defined by (44), (47), (52) determine the second-order solution with accuracy to an unknown function κ, say, describing free oscillations of the gas. In § 3.1, we have shown that such a function satisfies the homogeneous problem. No attempt will be made to calculate the function κ, though its effect on the solution will be discussed later on.

Using (51), one can characterize the resonance ($T_1 = 0$), pre-resonance ($T_1 < 0$) and post-resonance ($T_1 > 0$) gas oscillations in terms of the parameter τ_*. Thus, the resonance oscillations correspond to $\tau_* = 0$, and the pre-resonant and post-resonance oscillations to $\tau_* \in [-1, 0]$ and to $\tau_* \in [0, 1]$, respectively. Hence, the shock waves begin and end when $\tau_* = -1$ and $\tau_* = 1$, respectively. Our model predicts that the phase lag of shock reflection from the plug changes by 2π radians when the driving frequency increases from the lower bound of the resonance band, $\tau_* = -1$, to its upper bound, $\tau_* = 1$. Other properties of the solution are discussed in the following sections.

4. Numerical solution

To verify the analytical solution, we solve numerically the problem of resonance gas oscillations. We use an implicit finite difference algorithm of Beam & Warming (1976). This algorithm has been successfully used for many applications, including continuous flows and flows with shock waves (Anderson, Tannehill & Pletcher 1984). We solve (1) with $\tilde{q}_0 = 0$ for the adiabatic problem, and (1*a*, *b*) and (5) for the isentropic problem. In both cases, we impose the boundary conditions (9) and the laws of piston motion given by either (7) or (8). It is important to stress that the numerical solution intrinsically satisfies the conditions on the shock wave front, rendering it a good tool for the verification of the analytical model.

The accuracy of the algorithm is of $O(\Delta\tilde{x}^2)$ in space, and $O(\Delta\tilde{t})$ in time. We use a grid with a spatial step of $\Delta\tilde{x} = \tilde{x}_p(\tilde{t})/800$, and a time marching step of $\Delta\tilde{t} = 5\times10^{-4}\tilde{T}$. To test the grid quality, its density was increased, and it was found that an increase

in grid density hardly affects the accuracy of the solution. The homogeneous state is used as an initial condition of the simulation. The simulation is continued until a time-periodic solution is obtained.

5. Results and discussion

5.1. *Riemann invariants*

In the majority of previous studies, analytical solutions of the isentropic problem were obtained in terms of the Riemann invariants (see, for example, Whitham 1974). These invariants are

$$\frac{2}{\gamma-1}\rho^{(\gamma-1)/2} \pm u = \text{const} \quad \text{on} \quad \frac{\mathrm{d}X}{\mathrm{d}t} = u \pm \rho^{(\gamma-1)/2}. \tag{53}$$

This relation means that a combination of the hydrodynamic density and velocity is conserved on the characteristic. Equation (53) holds for flows without shocks, while for a flow with a weak shock wave, equation (53) is accurate up to the first order of the Mach number only (Whitham 1974). Chester (1964) proposed an extension of (53) accounting for the second-order terms.

In order to emphasize the physical meaning of our solution, we express it in terms of the Riemann invariants. We introduce new variables:

$$Z = z + \varepsilon\frac{3-\gamma}{4}f(y) + \varepsilon\frac{\gamma+1}{2}xf'(z), \tag{54a}$$

$$Y = y + \varepsilon\frac{3-\gamma}{4}f(z) + \varepsilon\frac{\gamma+1}{2}xf'(y). \tag{54b}$$

Substitution of the right-wave solution (38a, b) and (44a, b) into the invariants (53) leads to

$$\frac{2}{\gamma-1}\rho^{(\gamma-1)/2} + u = \frac{2}{\gamma-1} - 2\varepsilon f'(Y) - \frac{3-\gamma}{4}\varepsilon^2[f'(Y)]^2 + \varepsilon^2 C_\rho, \tag{55a}$$

$$\frac{2}{\gamma-1}\rho^{(\gamma-1)/2} - u = \frac{2}{\gamma-1} - 2\varepsilon f'(Z) - \frac{3-\gamma}{4}\varepsilon^2[f'(Z)]^2 + \varepsilon^2 C_\rho. \tag{55b}$$

Comparing this solution with that of Chester (1964), we see that in Chester's solution the terms of order ε^2 are absent. Hence, the Chester model describes the characteristics Z and Y, and the invariants with accuracy of the first order in ε only. The nonlinear terms of (55), which stem from condition (10a, b) on the shock wave front and global mass conservation (11), have not been considered until now. We demonstrate the effect of these terms on the solution in the following section.

Equation (55) presents an expansion of the Riemann invariants in terms of a small parameter ε. We introduce a new function

$$R(s) = \frac{2}{\gamma-1}\left(1 + as + \frac{\gamma-1}{2b}\varepsilon^2 C_\rho\right)^b, \tag{56a}$$

where

$$a = -\frac{3\gamma-1}{4}, \tag{56b}$$

$$b = 4\frac{\gamma-1}{3\gamma-1}. \tag{56c}$$

Using this function, we rewrite the invariants as

$$\frac{2}{\gamma-1}\rho^{(\gamma-1)/2}+u=R[\varepsilon f'(Y)], \tag{57a}$$

$$\frac{2}{\gamma-1}\rho^{(\gamma-1)/2}-u=R[\varepsilon f'(Z)]. \tag{57b}$$

To obtain an analytical solution, which is accurate up to the second order in ε, one should calculate $f(\tau)$ and C_ρ, and substitute them into (54), (56) and (57). For a particular case of sinusoidal piston motion $x_p^{(2)}(\tau)=-\cos\pi(\tau-\tau_*)$, we obtain $f(\tau)$ and C_ρ as

$$f(\tau)=\frac{T_1(\tau_*)}{\gamma+1}(1+\tau)-\frac{4}{\pi^{3/2}\sqrt{\gamma+1}}(\cos\pi(\tau-\tau_*)/2+\sin\pi\tau_*/2), \tag{58a}$$

$$C_\rho=\frac{8(1-\cos\pi\tau_*)}{\pi^3}+\frac{(\gamma-3)(\pi^2-4+4\cos\pi\tau_*)}{2\pi^3(\gamma+1)}, \tag{58b}$$

where

$$T_1(\tau_*)=\frac{4\sqrt{\gamma+1}}{\pi^{3/2}}\sin\left(\frac{\pi\tau_*}{2}\right). \tag{58c}$$

The shock wave coordinate $X(\tau)$ is

$$X(\tau)=\begin{cases}\tau+\varepsilon k[\sin(\pi\tau-\pi\tau_*/2)+(1+2\tau)\sin(\pi\tau_*/2)], & 0<\tau<1,\\ -\tau-\varepsilon k[\sin(\pi\tau-\pi\tau_*/2)+(1-2\tau)\sin(\pi\tau_*/2)], & -1<\tau<0,\end{cases} \tag{59a}$$

where

$$k=\frac{3-\gamma}{\pi^{3/2}\sqrt{\gamma+1}}. \tag{59b}$$

The left-wave solution can be obtained from the right-wave solution by the substitutions $(y\to y-2)$ and $(z\to z+2)$ into (54), for $0<\tau<2$ and $-2<\tau<0$, respectively.

Using (21), we write the vibrational frequency in the form

$$f=\frac{2f_{res}}{2+\varepsilon T_1(\tau_*)}, \tag{60}$$

where $T_1(\tau_*)$ is given by (58*c*) for a sinusoidally oscillating piston. Using (58*c*), (60), we define a resonance band as $f_{min}<f<f_{max}$, where

$$f_{min}=f_{res}\left(1+\frac{2\sqrt{\gamma+1}}{\pi^{3/2}}\varepsilon\right)^{-1},\quad f_{max}=f_{res}\left(1-\frac{2\sqrt{\gamma+1}}{\pi^{3/2}}\varepsilon\right)^{-1}. \tag{61}$$

We introduce a dimensionless frequency ϕ defined as $\phi=(f-f_{res})/\varepsilon f$. From (60) and (58*c*), we obtain

$$\phi(\tau_*)=-\frac{T_1(\tau_*)}{2}=-\frac{2\sqrt{\gamma+1}}{\pi^{3/2}}\sin\left(\frac{\pi\tau_*}{2}\right). \tag{62}$$

Hence, $\phi=0$ is equivalent to f_{res}, while the resonance band corresponds to the range $\phi_{min}\leqslant\phi\leqslant\phi_{max}$, where

$$\phi(-1)=\phi_{min}=-\frac{2\sqrt{\gamma+1}}{\pi^{3/2}},\quad \phi(1)=\phi_{max}=\frac{2\sqrt{\gamma+1}}{\pi^{3/2}}. \tag{63}$$

For air with $\gamma\approx1.4$, the resonance band is within $|\phi|\leqslant0.556$.

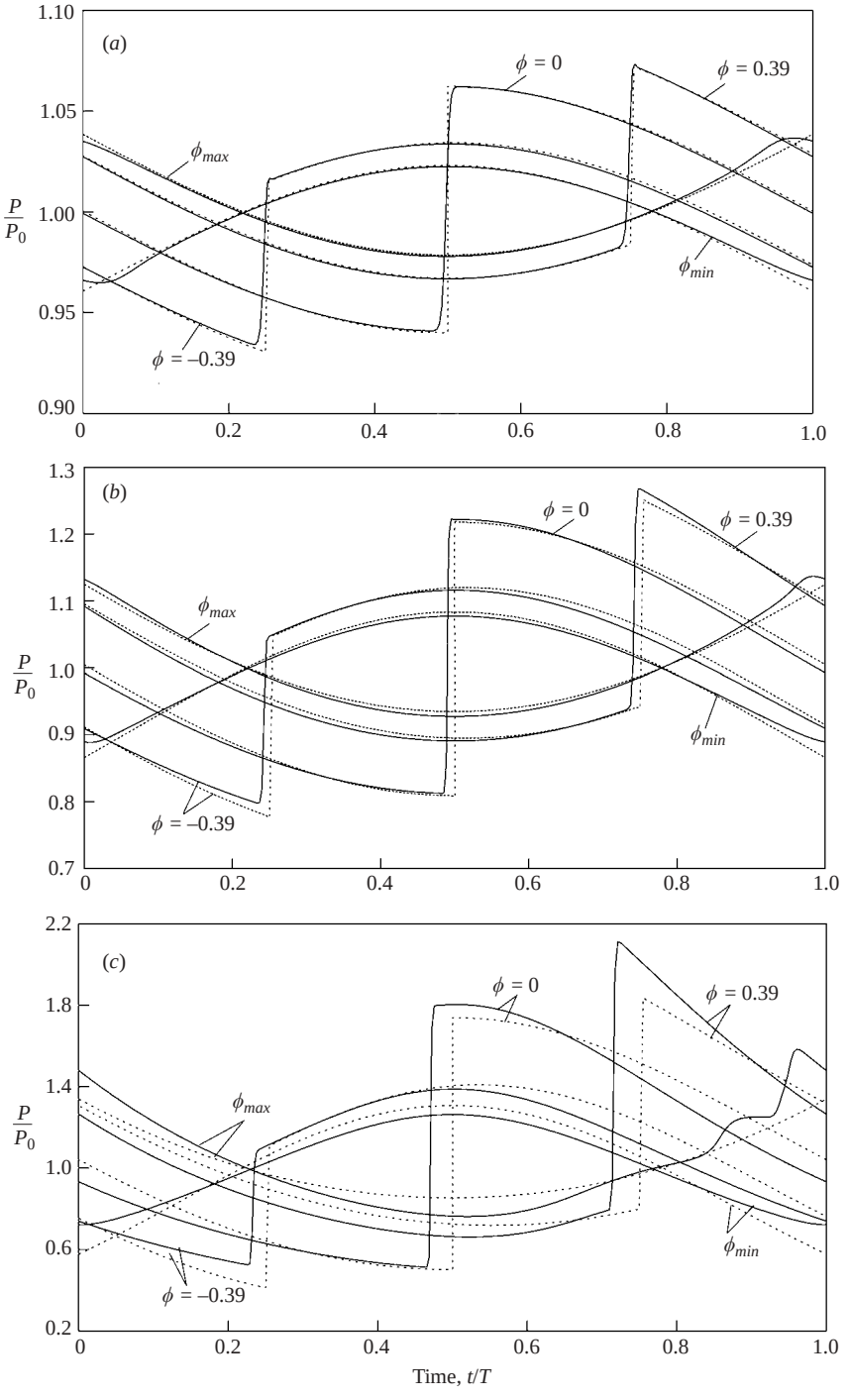

FIGURE 4. Time evolution of the pressure at the plug for a resonance tube with: (*a*) $\varepsilon = 0.03$; (*b*) $\varepsilon = 0.1$; (*c*) $\varepsilon = 0.3$. Dotted lines, theory; solid lines, numerical.

We use the analytical model of resonance gas oscillations to calculate the time evolution of gas pressure at the plug for a piston oscillating according to (7). Figures 4(*a*), 4(*b*) and 4(*c*) present model predictions in comparison with numerical

calculations for ε equal to 0.03, 0.1 and 0.3, respectively. In these figures, time is measured from the moment when the piston is in the instroke position. For the lower and upper bounds of the resonance band, corresponding to ϕ_{min} and ϕ_{max}, the pressure changes continuously without a jump. This means that no shock travels in the tube at these frequencies. However, there are abrupt pressure changes, which develop into shocks for frequencies within the resonance band. Thus, shocks appear at $\phi = 0$ and $\phi = \pm 0.39$, corresponding to $\tau_* = 0$ and $\tau_* = \mp 0.5$, respectively. We see in figure 4 that the phase lags $\varphi = \pi(1 - \tau_*)$ between the piston instroke position and the shock reflection from the plug are $\varphi(\phi_{min}) = 0$, $\varphi(-0.39) = \pi/2$, $\varphi(0) = \pi$, $\varphi(0.39) = 3\pi/2$ and $\varphi(\phi_{max}) = 2\pi$. Hence, φ changes by 2π radians, when the frequency is increased from ϕ_{min} to ϕ_{max}.

Figure 4(*a*) shows that for $\varepsilon = 0.03$, the analytical model fits the numerical results very well for all ϕ. The curves practically coincide everywhere except in the vicinity of the shock. Here, the deviation of the numerical model from the analytical one is because the numerical model suffers from shock spreading caused by spatial discretization. This spread is especially noticeable when the shock wave is weak as it is in the case $\varepsilon = 0.03$. For $\varepsilon = 0.1$ (figure 4*b*), a discrepancy between the analytical and numerical models can be observed. In particular, the models predict a different time of shock reflection from the plug: the numerical model predicts that the shock reflects somewhat before that predicted by the analytical model. The discrepancy arises because of the asymptotic nature of the analytical model, which is of the second order in ε. Still, for $\varepsilon = 0.1$, the agreement between the models is good. For $\varepsilon = 0.3$ (figure 4*c*), the discrepancies in pressure magnitude and shock reflection time between the models are significant, with the deviation being of the order of about ε^3. Hence, we conclude that the analytical model predicts the time of shock reflection with accuracy of ε^2, supporting the validity of (21). We also note that the difference in the pressure magnitude between the models is larger for the post-resonance frequencies. At $\phi = 0.39$, the shock amplitude predicted by the numerical model exceeds that of the analytical model by about 30%, as well as that at $\phi = 0$. The analytical model predicts maximum pressure jump at $\phi = 0$.

The dimensionless pressure amplitude on the tube plug $\Delta P/(\varepsilon P_0)$, where $\Delta P = P_{max} - P_{min}$, is shown in figure 5. We see that the pressure amplitude has a maximum inside the resonance band and sharply decreases near the resonance band bounds. For $\varepsilon = 0.03$ and $\varepsilon = 0.1$, the numerically calculated pressure amplitude is in good agreement with that obtained analytically, while for $\varepsilon = 0.3$, a notable discrepancy exists. For $\varepsilon = 0.3$, the analytical ΔP exceeds that calculated numerically for the pre-resonance frequencies, $\phi < 0$, and underestimates it for the post-resonance frequencies, $\phi > 0$, for which the difference is most significant.

In order to understand the cause of the large discrepancy between the models at $\phi > 0$, we calculate numerically the pressure amplitude ΔP for a wide frequency range. Figure 6 shows $\Delta P/(\varepsilon P_0)$ versus the dimensionless vibrational frequency f/f_{res}, for ε equal to 0.03, 0.1 and 0.3. For $\varepsilon = 0.03$ and $\varepsilon = 0.1$, there are sharp maxima of ΔP in the vicinity of $f/f_{res} = 1$, while for larger f/f_{res} the pressure amplitudes steadily decrease. In the case of $\varepsilon = 0.3$, the resonance band around $f/f_{res} = 1$, is significantly wider than for $\varepsilon = 0.03$ and $\varepsilon = 0.1$, because the resonance band width is proportional to ε (see (61)). Moreover, for $\varepsilon = 0.3$, additional local maxima exist at $f/f_{res} \sim 1.33$ and $f/f_{res} \sim 1.5$. The numerical simulations show that for these frequencies sub-resonance gas oscillations are excited. In figure 7, we present the time evolution of the pressure at the plug for $f/f_{res} = 1.5$ and $\varepsilon = 0.3$. The pressure oscillates with a periodicity equal to 3 piston periods. One can see that six interactions between the plug and the

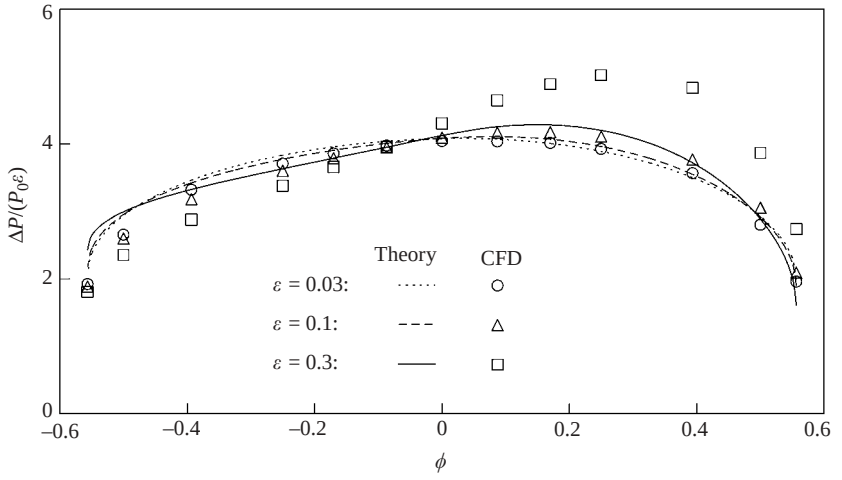

FIGURE 5. Dimensionless pressure amplitude $\Delta P/(\varepsilon P_0)$ within the resonance band versus dimensionless frequency ϕ for tubes with different ε.

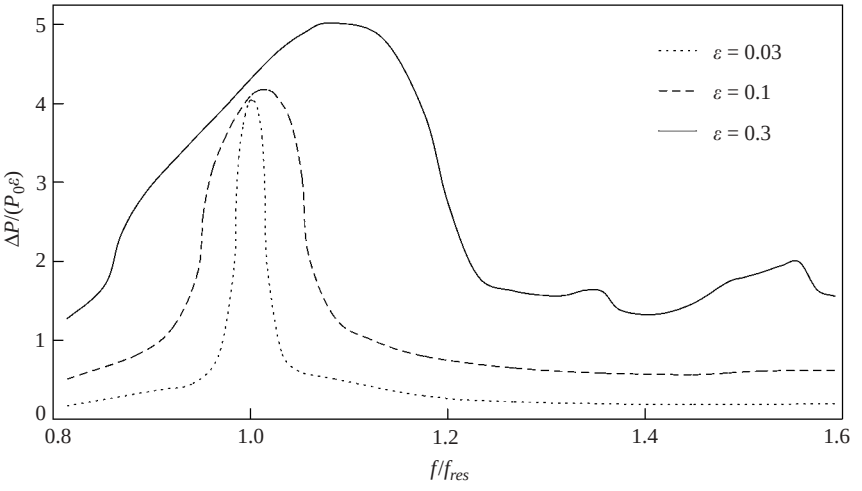

FIGURE 6. Dimensionless pressure amplitude $\Delta P/(\varepsilon P_0)$ versus dimensionless frequency f/f_{res}, where f_{res} is the first resonance frequency, for tubes with different ε.

shock take place during one pressure period. This means that two shock waves travel in the resonance tube simultaneously when $f/f_{res} = 1.5$. This result can be described theoretically using our approach. Rather than present a full description here, we delineate the main stages only.

As mentioned above, the function κ describes free oscillations of the gas of order ε^2. Bearing this in mind and the results of numerical simulations, this function can be presented as a superposition of (discontinuous) functions with periods $T/T_{res} = 1+1/n$, where $n = 2, 3, \ldots$. By doing so all sub-harmonic shock waves can be investigated by the method described in § 3. The resulting equations for the function κ can be found on the basis of periodicity, boundary, shock wave and global mass conservation

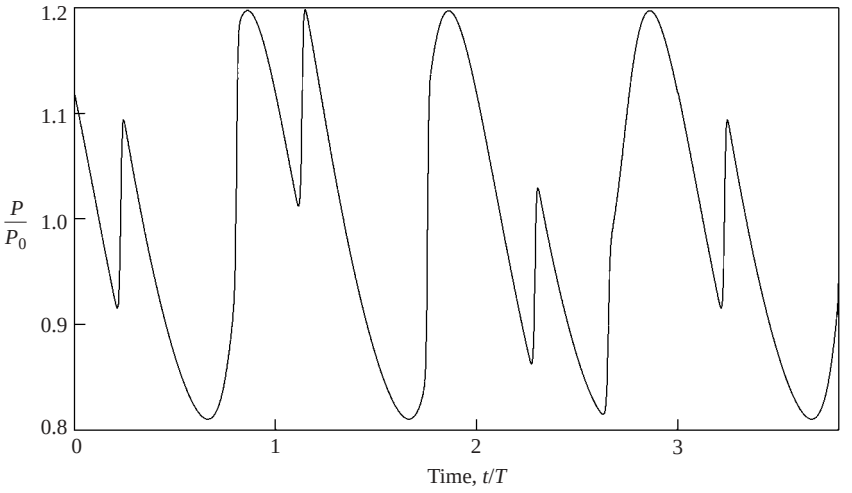

FIGURE 7. Time evolution of the pressure at the plug for a tube with $\varepsilon = 0.3$ and vibrational frequency $f/f_{res} = 1.5$, where f_{res} is the first resonance frequency.

conditions. After cumbersome calculations, the resulting equations of order ε^3 can be derived.

However, such an approach is of a more academic than practical interest, since the effect of sub-harmonic resonance oscillations is significant for large ε only. It should be noted that $\varepsilon = 0.3$ corresponds to a piston velocity of about $100\,\mathrm{m\,s^{-1}}$. To the best of our knowledge, no resonance tube has yet been built that would provide such high velocities.

5.2. *Average hydrodynamic properties*

In this subsection, we calculate the average heat and pressure distributions along the tube caused by periodic shock waves. Such distributions were first addressed by Merkli & Thomann (1975*b*). They stated that prediction of these distributions "should be possible by an extension of Chester's (1964) theory". In § 5.1, we showed the additional second-order terms, which do not appear in Chester's solution. Below we assess the effect of these terms on the time-average values.

For any hydrodynamic property Γ, one can calculate a time-average value in a cross-section with coordinate x as follows:

$$\langle \Gamma \rangle_t \equiv \frac{1}{T}\left\{ \int_{-T/2}^{t_-(x)} \Gamma_l \,\mathrm{d}t + \int_{t_+(x)}^{t_-(x)} \Gamma_r \,\mathrm{d}t + \int_{t_+(x)}^{T/2} \Gamma_l \,\mathrm{d}t \right\}, \tag{64a}$$

where Γ_l and Γ_r are the left- and right-wave values of Γ, and $t_-(x)$, $t_+(x)$ are the moments when the shock reaches coordinate x. These moments can be expressed in terms of the function $f(x)$ as

$$t_+(x) = x + \varepsilon\frac{T_1}{2}x - \varepsilon\frac{(3-\gamma)}{4}f'(2x-1), \tag{64b}$$

$$t_-(x) = -x - \varepsilon\frac{T_1}{2}x - \varepsilon\frac{(3-\gamma)}{4}f'(1-2x). \tag{64c}$$

The time-average hydrodynamic properties can be rewritten in terms of a function $g(x)$ as follows:

$$\frac{\langle\rho\rangle_t - \rho_0}{\rho_0\varepsilon^2} = (3-\gamma)g(x), \tag{65a}$$

$$\frac{\langle P\rangle_t - P_0}{P_0\varepsilon^2} = \gamma\left[g(x) + \frac{\gamma-1}{2}g(0)\right], \tag{65b}$$

$$\frac{\langle\theta\rangle_t - \theta_0}{\theta_0\varepsilon^2} = \frac{\gamma-1}{2}[g(x) + (\gamma-2)g(0)]. \tag{65c}$$

Here, the function $g(x)$ is given by

$$g(x) = \int_{-x}^{x} f'(y)f'(z)\,\mathrm{d}t + \int_{x}^{2-x} f'(y-2)f'(z)\,\mathrm{d}t$$
$$= \int_{-1}^{1-2x} f'(\zeta)f'(\zeta+2x)\,\mathrm{d}\zeta + \int_{1-2x}^{1} f'(\zeta)f'(\zeta+2x-2)\,\mathrm{d}\zeta \tag{66}$$

and has the following properties:

$$g(x) = g(1-x), \quad g(0) = K, \quad \int_0^1 g(x)\,\mathrm{d}x = 0, \tag{67}$$

where the constant K is given by (46c). According to (67), the function $g(x)$ is symmetric within the interval $x \in [0, 1]$ and has a zero average. The latter property can be assessed by integration of (65a) over the tube length and taking into account mass conservation. It is important to stress that the mean pressure and temperature deviate from their initial values, P_0 and θ_0, respectively. Integrating (65b, c) over the tube length yields

$$\frac{\langle P\rangle_{t,x} - P_0}{P_0\varepsilon^2} = \frac{\gamma(\gamma-1)}{2}K, \tag{68a}$$

$$\frac{\langle\theta\rangle_{t,x} - \theta_0}{\theta_0\varepsilon^2} = \frac{(\gamma-1)(\gamma-2)}{2}K, \tag{68b}$$

where $\langle\rangle_{t,x}$ denotes averaging over an oscillation period and tube length. We see that the deviations of the average values are proportional to K yielding a physical meaning for this constant.

Bearing in mind that for most gases the adiabatic exponent γ is close to unity, one can use (65b, c) to compare thermal and pressure gradients. Estimating the ratio of these gradients as $2\gamma/(\gamma-1)$, we see that the thermal gradient is weaker than the pressure gradient. For example, for air with $\gamma \approx 1.4$, the pressure gradient is $2\gamma/(\gamma-1) \approx 7$ times higher than the thermal gradient.

Using (58a, c) and (66) for the particular case of sinusoidal piston motion, we obtain

$$g(x) = -\frac{4[4 - 4\cos\pi\tau_* - \pi^2\cos\pi x + 2\pi^2 x\cos\pi x + 2\pi\cos\pi\tau_*\sin\pi x]}{\pi^3(1+\gamma)}. \tag{69}$$

We now compare the theoretical predictions (65b, c) with the results of numerical simulations. Such comparisons for $f = f_{res}$ and different ε are presented in figures 8(a)

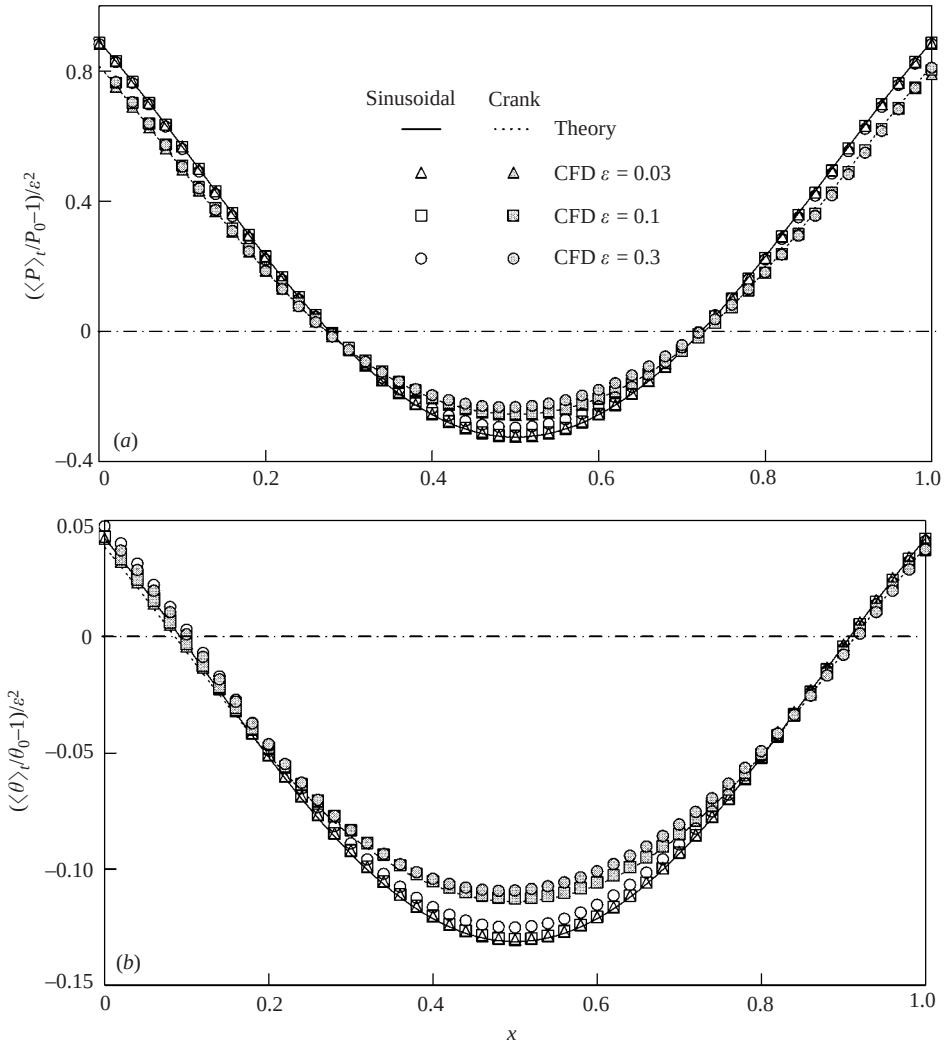

FIGURE 8. Time-average gas (*a*) pressure and (*b*) temperature versus dimensionless tube coordinate calculated for $f = f_{res}$ and different ε for sinusoidal or crank piston drives. The dash-dotted line is the prediction of Chester's theory.

and 8(*b*), where the time-average pressure and temperature are shown, respectively. The calculations are performed for two types of piston drive mechanisms; the first is the sinusoidal (7) and the second is the crank mechanism (8) with $\lambda = \frac{1}{3}$. The average pressure and temperature have a minimum at $x = 0.5$ and maximum values at the tube ends, which corresponds to experimental observations (Saenger & Hudson 1960; Merkli & Thomann 1975*b*; Zaripov & Ilhamov 1976). For $f = f_{res}$, the time-average pressure and temperature, calculated by the analytical model, agree with the numerical data for both drive mechanisms. Only a slight difference of less than 4% between the analytical and numerical modes is observed for ε as large as $\varepsilon = 0.3$.

In figure 8, we see that the time-average pressure and temperature depend on the type of piston drive mechanism. For the sinusoidal drive, the average values are larger than those for the crank mechanism by about 15%. Hence, by an appropriate

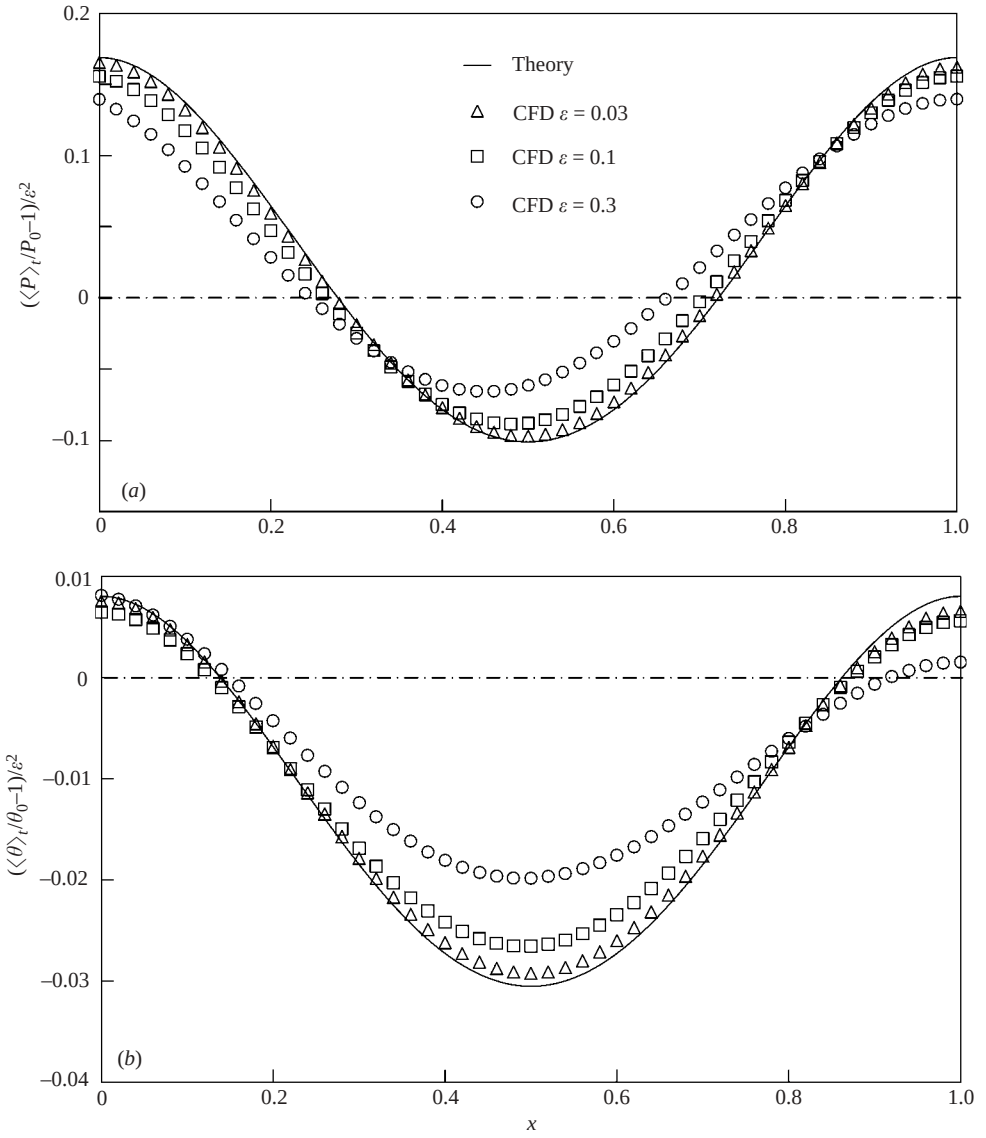

FIGURE 9. Time-average gas (a) pressure and (b) temperature versus dimensionless tube coordinate calculated for $f = f_{min}$ and different ε. The dash-dotted line presents the prediction of Chester's theory.

choice of the piston drive mechanism, any desired hydrodynamic gas properties can be obtained. This finding can be of importance in engineering practice.

We found that the most significant difference between the analytical and numerical models is at f_{min} and f_{max}. In figures 9(a) and 9(b), we present the average pressure and temperature, respectively, at $f = f_{min}$. It can be seen in these figures that the difference increases with increasing ε. This is due to the asymptotic nature of the theoretical model, which disregards terms of the third and higher orders affecting the average values. Our numerical model inherently accounts for the nonlinearity of gas flow. Hence, we use the numerical predictions to estimate the error of the theoretical

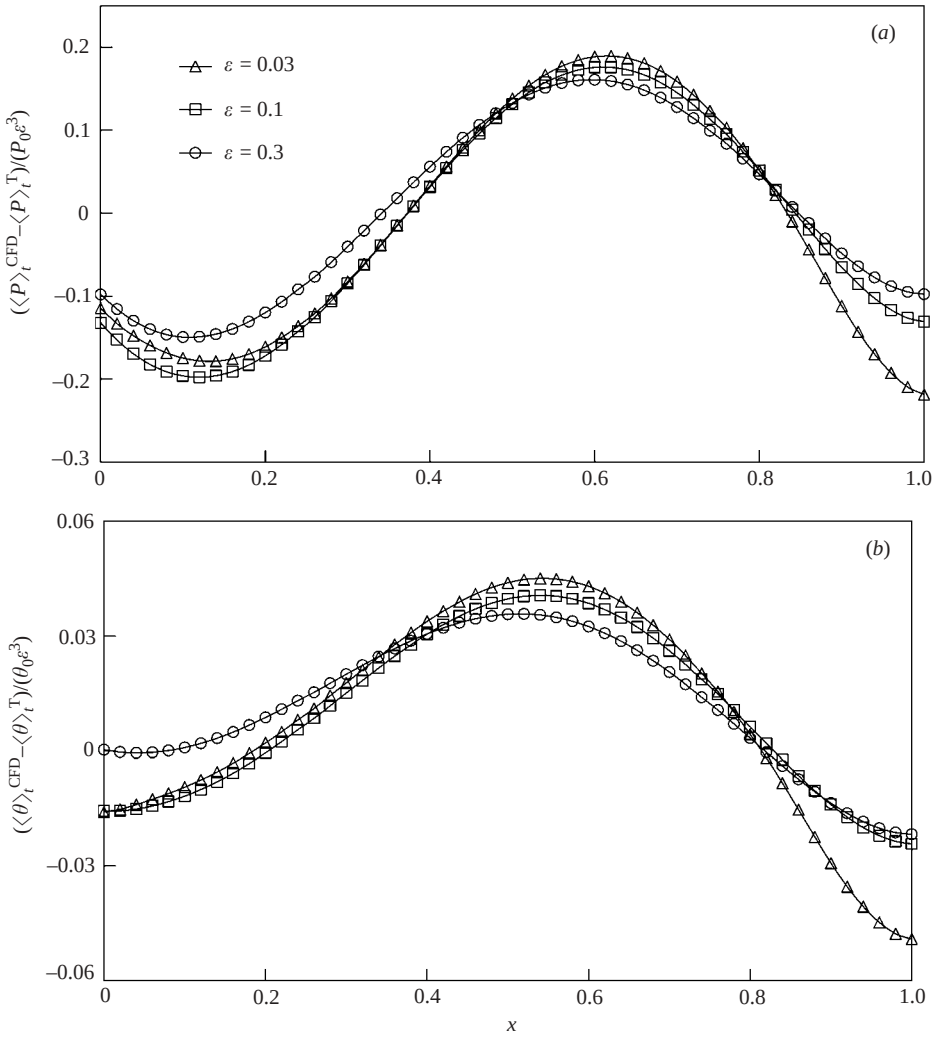

FIGURE 10. Time-average (*a*) pressure and (*b*) temperature difference between models versus dimensionless tube coordinate calculated for $f = f_{min}$ and resonance tubes with different ε; $\langle P\rangle_t$ and $\langle\theta\rangle_t$ – numerically (CFD) and analytically (T) calculated average pressures and temperatures, respectively.

model. Figures 10(*a*) and 10(*b*) present the theoretical model deviation from the analytical model for gas pressure and temperature for different ε. The curves are close to each other and of order of ε^3. Hence, the theory is accurate up to the order ε^2. The second-order terms are responsible for pressure and temperature gradients along the resonance tube. The prediction of the gradients for any frequency within the resonance band is one of the new results obtained in this work.

We calculate the hydrodynamic velocity averaged over a single vibrational period. Note that the analytical solution of the second order predicts zero average velocity, i.e.

$$\langle u\rangle_t = 0. \tag{70}$$

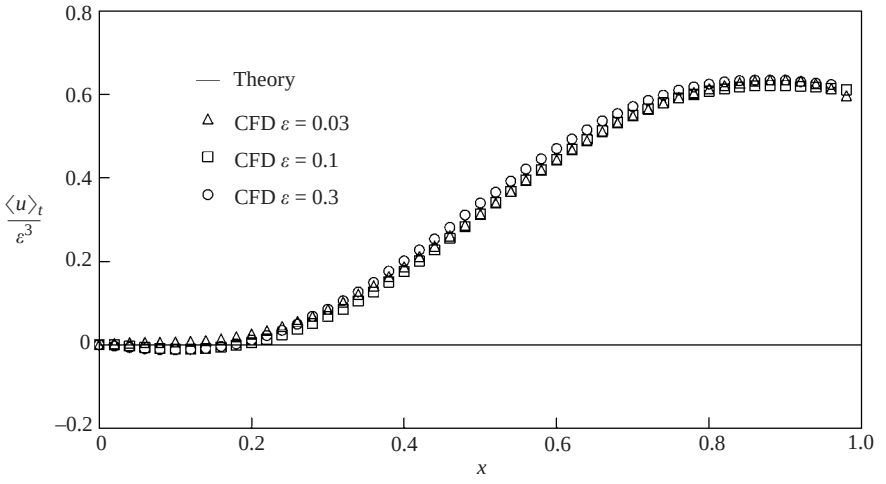

FIGURE 11. Time-average axial gas velocity versus dimensionless tube coordinate for $f = f_{res}$ and different ε.

Figure 11 presents the period-average gas velocity normalized by ε^3, which is calculated numerically for $f = f_{res}$. The average velocity caused by the gas compressibility is non-zero everywhere except in the vicinity of the plug. We see that the average velocity is of order of ε^3 and, therefore, cannot be predicted by our analytical model. It should be noted that $\langle \rho u \rangle_t$ is zero for both models, thus no permanent mass transfer occurs along the resonance tube.

5.3. *Energy balance*

The analytical solution of the problem of resonance gas oscillations disregards gas heating by assuming isentropic flow. In this section, we discuss a possible extension of the solution to a more practical case. We start from the calculation of energy generated by the vibrating piston. Using the expression for the right-side velocity and pressure, we calculate the energy generated by the piston per unit time and cross-section area as

$$E_p = -\frac{1}{T}\int_0^T Pu|_{x=1}\,\mathrm{d}t = \frac{(\gamma+1)}{12}[f'(1) - f'(-1)]^3\varepsilon^3, \tag{71a}$$

where

$$f'(1) - f'(-1) = A\sqrt{\frac{x_p^{(2)}(\pi - \pi\tau_*) - x_{in}^{(2)}}{2}} \tag{71b}$$

is the density jump at the shock wave given by (50). When $\tau_* = 0$ the jump is maximal, and zero when $\tau_* = \pm 1$.

In order to sustain periodic gas motion, external cooling $\tilde{q}_0$ (see (1c)) should be applied to the tube wall to continuously remove the heat generated by the work input to the piston. This means that $\tilde{q}_0 = \tilde{q}_p + \tilde{q}_{vis}$, where $\tilde{q}_p$ is the mechanical energy input from the vibrating piston to the inviscid gas by shock waves and $\tilde{q}_{vis}$ the viscous dissipation of the kinetic energy of the gas. In addition to these two modes of heat generation, there is also a heat interaction between the gas and the wall due to temperature variations in the gas, because of expansion and compression. This interaction does not enter the overall heat balance, because the heat removed from

the compressed gas is balanced by that added to the rarified gas, resulting in a net zero heat interaction (Merkli & Thoman 1975*b*).

Using equations (71), we obtain the heat generated by shock waves within the inviscid gas as

$$\tilde{q}_p = -E_p \tilde{\rho}_0 \tilde{C}_0^3 / \tilde{L}. \tag{72}$$

In the case $\tilde{q}_{vis} = 0$, the energy dissipated by the shock waves, E_{sh}, should be equal to that generated by the piston, E_p:

$$E_{sh} = E_p. \tag{73}$$

This energy balance condition was used by Betchov (1958) and Temkin (1968) for the closure of their models. It is easy to ascertain that (73) is identically satisfied in our model. To prove this, substitute (50) and (4) into relation (3) and compare the result with (71).

In the absence of cooling, the gas temperature in the tube increases continuously. In order to understand the thermal processes occurring in such a condition, we consider an inviscid adiabatic problem, in which no thermal interaction takes place between the gas inside the tube and the tube wall.

Aganin *et al.* (1996) accounted numerically for heat production. Their solution predicted aperiodic pressure changes and a rapid increase in gas temperature. We therefore explain the aperiodic nature of the adiabatic formulation as follows. Because of the adiabatic boundary, heat generated by the shock wave leads to a continuous increase in the average gas temperature $\bar{\theta}$, resulting in an increase in the speed of sound. As a result, the resonant frequency $f_{res}(\bar{\theta})$ and, accordingly, the resonance band are shifted towards the upper frequencies. The gas temperature continues to rise until the fixed piston frequency $f_p = f_{res}(\theta_0)$, becomes less than $f_{min}(\bar{\theta})$. Outside the resonance band there are no shocks and, hence, no heat generation.

From the linear resonance frequency definition, a relation between the dimensionless resonance frequency, f_{res}, and the dimensionless average temperature, $\bar{\theta}$, can be written as

$$\frac{f_{res}}{f_p} = \sqrt{\frac{\bar{\theta}}{\theta_0}}, \tag{74}$$

where $f_p = 1/2$ and $\theta_0 = 1$. As we show later, the time variation of $\bar{\theta}$ is of the third order in ε, and does not affect the second-order solution, which is derived in § 3 for a fixed average gas temperature with the oscillation frequency as a variable parameter. We now use the solution for a different problem where the oscillation frequency is fixed and the gas temperature changes. Substituting (21) into (74), and retaining the leading-order terms, we obtain

$$\bar{\theta} = 1 - \varepsilon T_1(\tau_*), \tag{75}$$

where the dependence of T_1 on τ_* arises from (51). Equation (75) indicates that the detuning function $T_1(\tau_*)$ describes the difference between the initial temperature $\tilde{\theta}_0$ and the current temperature, which changes due to gas heating. The parameter τ_* governs not only the temperature increase but also heat generation E_p via equations (71*a*, *b*). Equating the rate of temperature increase and heat generation, the equation of the energy balance is

$$\frac{\mathrm{d}T_1(\tau_*)}{\mathrm{d}\tau_1} = -\varepsilon^{-3} E_p(\tau_*), \tag{76}$$

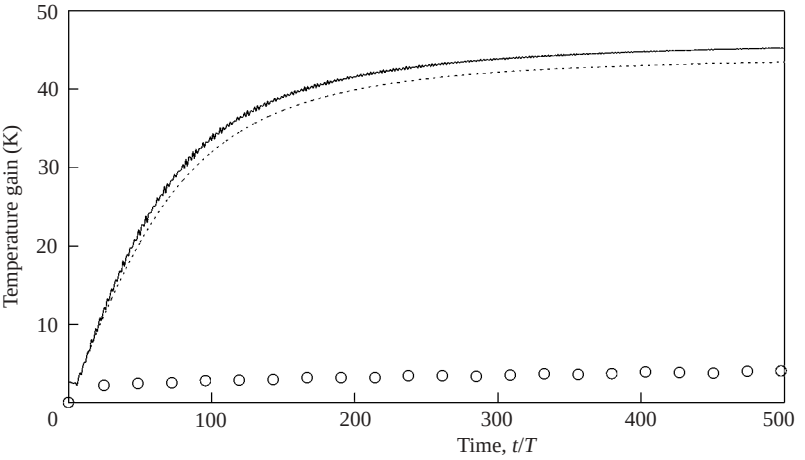

FIGURE 12. Temperature gain at the plug caused by a piston vibrating with $\tilde{f} = 47\,\mathrm{Hz}$ in a tube with $\varepsilon = 0.137$ versus the number of oscillation periods: dotted line – adiabatic analytical model (equation (78)); solid line – adiabatic numerical model; circles – experimental data of Alexeev *et al.* (2002).

where $\tau_1 = \varepsilon^2\tau$. Since E_p is of order ε^3 (see (71*a*)), the right-hand side of (76) is of the same order in ε as the left-hand side.

For the particular case of sinusoidal piston motion (7), $E_p(\tau_*)$ and $T_1(\tau_*)$ appearing in (71) and (51) can be expressed via elementary trigonometric functions, and equation (76) can be integrated to yield

$$\tau_1 = -\frac{3(\gamma+1)}{4}\tan\left(\frac{\pi\tau_*}{2}\right). \tag{77}$$

We combine (58*b*), (75) and (77) to obtain the time evolution of the gas temperature in the resonance tube as

$$\bar{\theta}(\tau) = 1 + \varepsilon\frac{4\sqrt{\gamma+1}}{\pi^{3/2}}\sin(z), \tag{78}$$

where $z = \tan^{-1}(\frac{4}{3}\varepsilon^2(\gamma+1)^{-1}\tau)$.

In figure 12, we compare the temperature predicted by the model (78) with numerical data for an adiabatic resonance tube. The calculation is performed for a resonance tube, $\tilde{L} = 367.7\,\mathrm{cm}$ long and 5.5 cm in internal diameter, which was used in the experiments of Alexeev *et al.* (2002). This tube can be characterized by $\varepsilon = 0.137$ and the first linear resonance frequency of about $\tilde{f}_{res} = 46.7\,\mathrm{Hz}$. As seen, the temperature increase calculated by (78) is in good agreement with the numerical simulation. The difference between the models does not exceed 5%. Initially, the temperature increase is rather vigorous since the piston frequency is close to the first linear resonance frequency, when the heat generation is most intensive. As the temperature increases, the resonance frequency goes up resulting in more minor heat generation. Now, the temperature increases slowly, till it approaches a constant, for which the piston frequency corresponds to the lower bound of the resonance band.

In the adiabatic analytical model, we assume a constant gas temperature during a single period. This assumption is verified by the numerical results (figure 12), where the temperature gain during one period does not exceed 0.5 °C. Hence, for times of the order of a single period, the adiabatic problem can be approximated by the

isentropic one. That is why we use the isentropic heat sink term of (73) to calculate the temperature gain in the adiabatic problem. The fact that the analytical results agree with the numerical model, attests to the relevance of this procedure.

In the adiabatic problem depicted in figure 12, we obtain a final temperature gain of about 45 °C. This result contradicts the experimental data of Alexeev *et al.* (2002), which show that the temperature gain is less than 3 °C. Moreover, the gas oscillations are practically periodic and remain within the resonance band throughout the duration of the experiment, because of a heat interaction between the gas and the tube. As a result of this interaction, all the heat generated during gas motion is removed, and, therefore, periodic gas oscillations are sustained. Hence, in such experimental conditions, resonance gas oscillations correspond to the pseudo-isentropic case, when $\tilde{q}_0$ is given by (73) for an inviscid gas.

Viscosity and thermal conductivity of a gas lead to additional heat effects in the viscous boundary layer. To obtain some knowledge about these effects, we consider a particular case of gas oscillation in a resonance tube characterized by the following conditions: (i) the thickness of the Stokes boundary layer is small compared to the tube radius; (ii) the wall temperature is constant; (iii) the piston frequency is outside the resonance band. For this special case, Rott (1980) calculated the thermal exchange between the boundary layer and the core flow caused by acoustic streaming in the form

$$\tilde{Q}_{bound} = \tilde{\rho}_0 \tilde{C}_0^3 (k_1 + k_1 k_2 \cos(2\pi x))\varepsilon^2, \tag{79a}$$

where

$$k_1 = A^2 \left(1 + \frac{\gamma - 1}{\sqrt{Pr}}\right) \sqrt{\frac{\pi \tilde{\nu}}{8 \tilde{L} \tilde{C}_0}}, \tag{79b}$$

$$k_2 = \frac{\gamma(1 + Pr) + (1 - Pr)(1 + \sqrt{Pr})}{\gamma(1 + Pr) - (1 + Pr)(1 - \sqrt{Pr})}; \tag{79c}$$

here $\tilde{\nu}$ is the gas kinematic viscosity and Pr is the Prandtl number.

Equation (79) indicates that the heat flux through a unit area of the tube wall $\tilde{Q}_{bound}$ consists of two parts: a constant and an alternating flux along the tube. The constant part describes gas heating, while the alternating one denotes gas cooling around the middle cross-section of the tube and heating around the tube ends. Bearing in mind that the second term does not change the total energy of the gas, the heating caused by gas viscosity can be written in the form

$$\tilde{q}_{vis} = 4 k_1 \varepsilon^2 \tilde{\rho}_0 \tilde{C}_0^3 / \tilde{d}, \tag{80}$$

where $\tilde{d}$ is the tube diameter. Comparison of this heat source with that obtained for an inviscid gas (see (71), (72)) under resonance yields

$$\frac{\tilde{q}_{vis}}{\tilde{q}_p} = \frac{4 k_1 \varepsilon^2}{E_p} \frac{\tilde{L}}{\tilde{d}} = \frac{48}{(\gamma + 1) A^3} \frac{k_1 \tilde{L}}{\varepsilon \tilde{d}}. \tag{81}$$

For typical experimental conditions, this ratio is less than 1. For example, for the experiments of Alexeev *et al.* (2002) $\tilde{q}_{vis}/\tilde{q}_p$ it is about 0.6. The second term of the heat flux, $\tilde{Q}_{bound}$, which accounts for acoustic streaming, leads to a pressure gradient along the tube wall, in the form

$$\Delta P_{acous} = 4 k_1 k_2 \varepsilon^2 (\tilde{L}/\tilde{d}) t \cos(2\pi x). \tag{82}$$

This expression can be compared with the inviscid one of (65*b*), (69). Both are of second order with respect to ε, and have similar profiles with a minimum in the middle cross-section and maxima at the tube ends. The most important difference between these two cases is that the inviscid pressure gradient is independent of time and tube diameter, while the viscous one increases linearly with time and strongly depends on the tube diameter. It is instructive to compare the pressure amplitudes (i.e. differences between the maximal and minimal values of pressure along the tube) of both profiles. Simple calculations yield the following linear time dependence:

$$\frac{\Delta P_{acous}}{\Delta P_{sh}} = \frac{2\pi^2(\gamma+1)k_1k_2\tilde{L}}{(2+\pi)\gamma\tilde{d}}t. \tag{83}$$

For typical experimental conditions, the prefactor in equation (83) is small. For example for experimental conditions of Alexeev *et al.* (2002) $\Delta P_{acous}/\Delta P_{sh} \approx 0.1t$. This means that the inviscid pressure gradient dominates for times of the order of the resonance period, while the viscous one dominates for large times.

In fact, heat and viscous interactions reduce the amplitude of gas oscillations (Alexeev *et al.* 2002). Hence, these interactions should be incorporated into the analysis of gas oscillations. These interactions are most pronounced in the case of turbulent gas flow. Merkli & Thomann (1975*a*) found that the onset of turbulence occurs outside the resonance band, where no shocks exist. The critical Reynolds number $Re_\delta = \hat{u}\sqrt{2/\nu\tilde{\omega}}$ above which the flow is turbulent, was found to be $Re_\delta^{crit} = 283$. Here, $\hat{u}$ is the axial velocity amplitude. Based on this result, Alexeev & Gutfinger (2003) obtained a criterion for the critical tube parameter as

$$\varepsilon_{crit} \approx \frac{Re_\delta^{crit}}{1.4}\sqrt{\frac{\pi\nu}{2\tilde{C}_0\tilde{L}}}.$$

When $\varepsilon < \varepsilon_{crit}$, gas flow at resonance is laminar and when $\varepsilon > \varepsilon_{crit}$, it is turbulent. For $\varepsilon > \varepsilon_{crit}$, an ad-hoc numerical model was proposed by Alexeev *et al.* (2002). More recently, Alexeev & Gutfinger (2003) treated gas oscillations in a resonance tube numerically, using the turbulence model of Wilcox (1993). Unfortunately, no analytical solution of turbulent gas oscillations in a resonance tube exists to date. Hence, we cannot extend our analytical model to the case of turbulent viscous flow. For tubes with $\varepsilon < \varepsilon_{crit}$, where the flow is laminar, the viscous terms can be included into our analytical model as suggested by Chester (1964). In a similar way the effect of heat interaction between the gas and the tube wall may be incorporated into the analytical model, thereby extending it to the case of adiabatic resonance oscillations of a viscous gas. The treatment of this problem is left for a future work.

6. Conclusions

An analytical model of inviscid gas oscillation inside a resonance tube was derived for an arbitrary law of piston motion. The model describes gas oscillations within a resonance band about the linear resonance frequency f_{res}, in which gas flow is accompanied by a shock wave propagating periodically back and forth along the tube. The model was obtained by a perturbation method accounting for terms of the second order of a small parameter $\varepsilon = \sqrt{\pi\tilde{l}/\tilde{L}}$. We have shown that some second-order terms were omitted in the previous works. These terms affect the model prediction of spatial gradients of the time-average gas temperature, pressure and density. Such temperature gradients were measured earlier by Merkli & Thomann (1975*b*). We

found that the gradients are controlled by the law of piston motion, and strongly depend on the value of the adiabatic exponent γ of the gas.

The isentropic and adiabatic problems were considered. Under adiabatic boundary conditions, the gas is heated continuously by irreversible energy dissipation through the shock wave. As a result, the average gas temperature increases steadily resulting in aperiodic gas oscillations. After some time, the oscillation frequency moves out of the resonance band and the flow becomes continuous. An analytical description of the aperiodic gas oscillations was obtained, leading to an expression for the average temperature evolution.

In parallel, a numerical model of resonance gas oscillation was developed. Since the numerical model intrinsically accounts for the nonlinearity of gas flow, we used the numerical solution to verify our analytical model. We considered two types of piston drive: a pure sinusoidal oscillator (7), and a crank mechanism (8). We compare different instantaneous and average hydrodynamic gas parameters. Good agreement was obtained between the analytical and numerical models everywhere in the resonance band. It was shown that the discrepancies between the models are of the order of ε^3. Hence, we conclude that the accuracy of the analytical model is of the order of ε^2.

We found numerically that for $\varepsilon = 0.3$, gas motion about the first resonance is affected by the resonances at $f/f_{res} = 1.33$ and $f/f_{res} = 1.5$. The existence of such resonances, when two shock waves travel simultaneously, has not been reported before and, hence, it requires further investigations. Our analytical model disregards these additional resonances that increase the discrepancy between the models for $\varepsilon = 0.3$. However, this discrepancy is of the order of ε^3.

For the case of adiabatic oscillations, the temperature gain predicted by the analytical model was compared with numerical data, resulting in good agreement. For typical experimental conditions, the temperature gain is significantly less than that calculated from the adiabatic model, because of heat interactions between the gas and the tube. Experiments show that such interactions remove practically all the heat dissipated within the tube, and lead to a constant average gas temperature corresponding to the pseudo-isentropic problem formulation. For this case, the amount of heat to be removed from the inviscid gas was calculated. For the case of laminar gas flow at $\varepsilon < 0.1$, the analytical model may be further extended to incorporate terms accounting for the effect of viscous and heat interactions between the gas and the tube.

Partial support of this work by the Israel Science Foundation, grant no. 53/01 is gratefully acknowledged.

REFERENCES

Aganin, A. A., Ilgamov, M. A. & Smirnova, E. T. 1996 Development of longitudinal gas oscillations in a closed tube. *J. Sound Vib.* **159**, 359–374.

Alexeev, A., Goldshtein, A. & Gutfinger, C. 2002 Heat interaction in a resonance tube. *Phys. Fluids* **14**, 1812–1815.

Alexeev, A. & Gutfinger, C. 2003 Resonance gas oscillations in closed tubes – numerical study and experiments. *Phys. Fluids* **15**, 3397–3408.

Anderson, D. A., Tannehill, J. C. & Pletcher, R. H. 1984 *Computational Fluid Mechanics and Heat Transfer*. Hemisphere.

Beam, R. M. & Warming, R. F. 1976 An implicit finite-difference algorithm for hyperbolic systems in conservation law form. *J. Comput. Phys.* **22**, 87–110.

Betchov, B. 1958 Non-linear oscillations of the column of a gas. *Phys. Fluids* **1**, 205–212.

Chester, W. 1964 Resonant oscillations in closed tubes. *J. Fluid Mech.* **18**, 44–64.

Galiev, S. U., Ilgamov, M. A. & Sadykov, A. V. 1970 On periodic shock waves in a gas. *Fluid Dyn.* **5**, 223.

Goldshtein, A., Vainshtein, P., Fichman, M. & Gutfinger, C. 1996 Resonance gas oscillations in closed tubes. *J. Fluid Mech.* **322**, 147–163.

Gulyaev, A. I. & Kuznetsov, V. M. 1963 Large amplitude gas oscillations in a closed tube. *Ingenernyi Zh.* **3**, 236–245.

Ilgamov, M. A., Zaripov, R. G., Galliulin, R. G. & Repin, V. B. 1996 Nonlinear oscillations of a gas in a tube. *Appl. Mech. Rev.* **49**, 137–154.

Ilinskii, Y. A., Lipkens, B. & Zabolotskaya, E. A. 2001 Energy losses in an acoustical resonator. *J. Acoust. Soc. Am.* **109**, 1859–1870.

Keller, J. 1976 Resonant oscillations in closed tubes: the solution of Chester's equation *J. Fluid Mech.* **77**, 279–304.

Lawrenson, C. C., Lipkens, B., Lucas, T. S., Perkins, D. K. & Van Doren, T. W. 1998 Measurements of macrosonic standing waves in oscillating closed cavities. *J. Acoust. Soc. Am.* **104**, 623–636.

Merkli, P. & Thomann, H. 1975*a* Transition to turbulence in oscillating pipe flow. *J. Fluid Mech.* **68**, 567–575.

Merkli, P. & Thomann, H. 1975*b* Thermoacoustic effects in a resonance tube. *J. Fluid Mech.* **70**, 161–177.

Rayleigh, Lord. 1945 *The Theory of Sound*. Dover.

Riley, N. 1997 Acoustic streaming. In *Encyclopedia of Acoustics* (ed. M. J. Croker), vol. 1, pp. 321–327. Wiley.

Riley, N. 2001 Steady streaming. *Annu. Rev. Fluid Mech.* **33**, 43–65.

Riley, N. & Trinh, E. H. 2001 Steady streaming in an oscillatory inviscid flow. *Phys. Fluids* **13**, 1956–1960.

Rott, N. 1974 The heating effect connected with non-linear oscillations in a resonance tube. *Z. Angew. Math. Phys.* **25**, 619–634.

Rott, N. 1980 Thermoacoustics. In *Advanced in Applied Mechanics*, 20, Chapter B. Isothermal Walls, 170–173

Saenger, R. A. & Hudson, G. E. 1960 Periodic shock waves in resonating gas columns. *J. Acoust. Soc. Am.* **32**, 961–971.

Shigley, J. E. & Uicker, J. J. 1995 *Theory of Machines and Mechanisms*. McGraw-Hill.

Shuster, K., Fichman, M., Goldshtein, A. & Gutfinger, C. 2002 Agglomeration of submicrometer particles in weak periodic shock waves. *Phys. Fluids* **14**, 1802–1805.

Sprenger, H. 1954 Über die thermische Effekte in Resonanzrohren. *Mitt. I.f.A.E., Eidgenössishe Technische Hochschule, Zürich*, No. 21, p. 18.

Sturtevant, B. B. 1974 Nonlinear gas oscillations in pipes. Part 2. Experiment. *J. Fluid Mech.* **63**, 97–120.

Temkin, S. 1968 Nonlinear gas oscillations in a resonance tube. *Phys. Fluids* **11**, 960–963.

Whitham, G. B. 1974 *Linear and nonlinear waves*. John Wiley & Sons.

Wilcox, D. C. 1993 *Turbulence Modeling for CFD*. La Canada.

Zaripov, R. G. & Ilhamov, M. A. 1976 Non-linear gas oscillations in a pipe. *J. Sound Vib.* **46**, 245–257.